RSC Advances

PAPER

View Article Online
View Journal | View Issue

Cite this: *RSC Adv.*, 2026, **16**, 30563

Anthocyanin-based intelligent food packaging films reinforced with ginger pseudostem cellulose fibers: a sustainable approach for real-time freshness monitoring of perishable foods

Nguyen Chi Thanh, †*[a] Pham Nguyen Hong Nhu,†[a] Nguyen Quoc Dat,[a] Bui Phuong Dong,[a] Nguyen Thanh Huy, [bc] Nguyen Bui Anh Duy [bc] and Nguyen Tue Anh[d]

This study aimed to fabricate a poly(vinyl alcohol) (PVA)-based intelligent indicator by combining anthocyanin-rich extracts from purple passion fruit peel (PPFP) with cellulose fibers extracted from ginger pseudostem (GP). Anthocyanins were obtained from PPFP *via* ultrasound-assisted extraction (UAE), achieving a maximum content of 1.53 mg cyanidin-3-*O*-glucoside equivalents (C3G)/g dry weight (DW) under optimized conditions. Cellulose fibers (CFs) extracted from GP through chemical treatment exhibited high purity, enhanced thermal stability, and a crystallinity index of 74.65%. The effects of anthocyanin incorporation and CF reinforcement at different levels on the structural characteristics, physicochemical properties, and pH-responsive color behavior of the films were evaluated. The result showed that the smart film reinforced with 1.0 wt% CFs exhibited reduced water vapor permeability (WVP), decreasing from 3.39 to 2.95 ($\times 10^{-10}$ g m^{-1} s^{-1} Pa^{-1}) compared to the film containing only anthocyanin. The mechanical properties of the films were enhanced upon the incorporation of anthocyanin and reinforcement with 1.0 wt% CFs, as evidenced by increases in tensile strength (from 21.09 to 32.21 MPa), elongation at break (from 261.06% to 404.68%), and Young's modulus (from 91.72 to 97.05 MPa). The practical applicability of the films was evaluated by monitoring the freshness of refrigerated shrimp, during which distinct color changes from pinkish-brown to green were observed in response to freshness deterioration. Overall, the developed intelligent films demonstrate strong potential for monitoring the freshness of perishable foods, including meat and seafood, thereby contributing to improved food quality assurance and consumer safety.

Received 22nd April 2026
Accepted 22nd May 2026

DOI: 10.1039/d6ra03420a

rsc.li/rsc-advances

1. Introduction

During food processing, distribution, and storage, product quality is highly susceptible to deterioration caused by environmental conditions, particularly temperature, humidity, and microbial activity.[1] The spoilage process is accompanied by the degradation of proteins and lipids, generating volatile compounds such as ammonia, trimethylamine, and organic acids.[2] These compounds cause undesirable changes in odor, color, and pH, ultimately compromising food quality and safety. Despite their widespread use, conventional petroleum-based packaging materials are non-biodegradable and function primarily as passive barriers, contributing to environmental pollution, microplastic formation, and potential chemical migration into food.[3,4] As promising alternatives, biodegradable polymers have gained significant attention for food packaging applications. Poly(vinyl alcohol) (PVA) stands out due to its non-toxicity, excellent film-forming ability, high biocompatibility, and biodegradability, making it suitable for food packaging applications. Recent studies have focused on improving the properties of biodegradable films through polymer blending or the incorporation of functional fillers, particularly toward the development of intelligent packaging systems capable of real-time food quality monitoring. This trend highlights the substantial potential of environmentally friendly packaging materials in the modern food industry.[5,6]

[a]*Faculty of Applied Sciences, Ho Chi Minh City University of Technology and Engineering, 01 Vo Van Ngan Street, Thu Duc Ward, Ho Chi Minh City, Vietnam. E-mail: thanhnc@hcmute.edu.vn; 21130086@student.hcmute.edu.vn; 21130006@student.hcmute.edu.vn; 20130020@student.hcmute.edu.vn*

[b]*Department of Polymer Materials, Faculty of Materials Technology, Ho Chi Minh City University of Technology (HCMUT), 268 Ly Thuong Kiet Street, Dien Hong Ward, Ho Chi Minh City, Vietnam. E-mail: nthuy.sdh241@hcmut.edu.vn; nbaduy.sdh241@hcmut.edu.vn*

[c]*Vietnam National University Ho Chi Minh City, Linh Xuan Ward, Ho Chi Minh City, Vietnam*

[d]*School of Science, Engineering & Technology, RMIT Saigon South, 702 Nguyen Van Linh Boulevard, Tan Hung Ward, Ho Chi Minh City, Vietnam. E-mail: anh.nguyen783@rmit.edu.vn*

† Contribution equal.

Purple passion fruit (*Passiflora edulis f. edulis*), a perennial climbing plant of the Passifloraceae family, originated in South America and is now widely cultivated in tropical and subtropical regions worldwide.[7] In the food industry, it is primarily consumed as fresh juice or processed products, generating a substantial amount of peel that accounts for approximately 62% of the total fruit weight.[8] Recent studies have demonstrated that purple passion fruit peel (PPFP) is a valuable source of bioactive compounds, particularly anthocyanins such as cyanidin-3-glucoside (C3G).[8,9] Anthocyanins are water-soluble polyphenolic pigments responsible for red to blue coloration in plant tissues[10] and are widely used as natural food colorants. More importantly, their pronounced pH-responsive color variation enables their application as colorimetric indicators.[11] This unique property has stimulated growing interest in the incorporation of anthocyanins into intelligent packaging systems, providing a sustainable and effective approach for real-time monitoring of food quality and freshness, particularly in perishable products.[12]

Ginger (*Zingiber officinale*) is a widely cultivated tropical and subtropical crop of the Zingiberaceae family, commonly used as both a culinary spice and medicinal plant. According to FAOSTAT data, global ginger production increased from approximately 4.3 million tons in 2020 to 4.9 million tons in 2023, with nearly 80% produced in Asia.[13] The global market for fresh and dried ginger is expected to continue expanding, particularly in the organic spice sector, where ginger essential oil is considered a high-value product with strong growth prospects toward 2030.[14] Despite its economic significance, substantial quantities of ginger pseudostems are generated during harvesting and processing and are typically discarded or underutilized. This inefficient utilization not only results in resource loss but also poses environmental concerns. Recent studies have reported that ginger pseudostems contain up to approximately 48% cellulose, along with hemicellulose, lignin, and other components.[15] Consequently, valorizing ginger pseudostem waste for cellulose extraction offers a promising approach to reduce agricultural residues while advancing sustainable material development and circular economy initiatives.

In this work, a novel dual by-product valorization strategy is proposed, whereby extracts from purple passion fruit peel and cellulose obtained from ginger pseudostem are simultaneously integrated into a poly(vinyl alcohol)-based intelligent film. By combining the intrinsic pH-responsive colorimetric properties of the natural extract with a biodegradable PVA matrix and cellulose fibers reinforcement, the developed film delivers multifunctional characteristics as a sustainable intelligent packaging material. The resulting intelligent films were comprehensively characterized in terms of their structural, physicochemical, and mechanical properties, as well as their pH-responsive color behavior. Furthermore, their practical applicability for real-time monitoring of freshness in perishable foods was demonstrated.

2. Materials and methods

2.1. Materials

Purple passion fruit (*Passiflora edulis f. edulis*) peels (PPFP) were thoroughly washed, cut into small pieces, frozen, and subsequently freeze-dried. After drying, the samples were ground into a fine powder to obtain the raw material for anthocyanins extraction. Ginger (*Zingiber officinale*) pseudostems were thoroughly washed, cut into small pieces, dried at 50 °C for 2 days, and mechanically ground. The resulting powder was sieved to obtain a uniform particle size. Shrimp samples were purchased from a local supermarket (Ho Chi Minh City, Vietnam). Absolute ethanol (≥99.5%), potassium chloride (KCl), sodium acetate (CH_3COONa), hydrochloric acid (HCl), sodium hydroxide (NaOH), hydrogen peroxide (H_2O_2), polyvinyl alcohol (PVA) (M_W, 60 000–125,000 g mol^{-1}), glycerol ($C_3H_8O_3$), sodium chloride (NaCl), calcium chloride ($CaCl_2$) were purchased from Sigma Aldrich.

2.2. Methods

2.2.1. Extraction of purple passion fruit peels (PPFP). The extraction conditions for anthocyanins from PPFP were optimized by systematically evaluating the effects of ethanol concentration (20–80%, v/v), solid-to-solvent ratio (1 : 15–1 : 30, w/v), and extraction time (5–45 min). The detailed extraction conditions were summarized in Tables S1–S3 of the Supplementary Information. To enhance anthocyanin stability, the extraction solvent was acidified with acetic acid to approximately pH 3. Ultrasound-assisted extraction was then performed, followed by vacuum filtration to obtain the extract. The resulting filtrate was concentrated under reduced pressure using a rotary evaporator at 40 °C and subsequently stored at low temperature under light-protected conditions prior to further analysis. Fig. 1a illustrated the extraction process of anthocyanins from purple passion fruit peel.

2.2.2. Preparation of cellulose fibers. The cellulose extraction process from ginger pseudostems consisted of two main stages: a pretreatment stage and a bleaching stage. The ginger pseudostem powder was treated with a 5% (wt/v) NaOH solution, followed by heating and continuous stirring at 80 °C for 1 h. After treatment, the solid residue was filtered and washed with distilled water until neutral pH (pH ≈ 7) was achieved. Subsequently, the pretreated sample was subjected to bleaching using a 10% (v/v) H_2O_2 solution, which was mixed with the pretreated sample at a ratio of 1 : 20 (wt/v) based on the initial mass of ginger pseudostem powder used. The mixture was continuously stirred at 90 °C for 2 h, while the pH was adjusted to approximately 11 using NaOH. The bleached sample was then filtered, thoroughly washed with distilled water, and freeze-dried for 48 h under a vacuum pressure below 30 Pa prior to further characterization. The cellulose fiber extraction process from ginger pseudostems was illustrated in Fig. 1b.

2.2.3. Preparation of films. The films were prepared using the solvent casting method. A 5% (wt/v) PVA solution was prepared by dissolving PVA in distilled water at 80–90 °C. Meanwhile, the cellulose suspension was prepared by accurately weighing the cellulose fibers according to each ratio, followed by dispersion in 5 mL of distilled water and ultrasonication for 5 min to obtain a homogeneous suspension. The cellulose suspension was then added to the 5% (wt/v) PVA solution and continuously stirred for 30–60 min. After the temperature of the mixture

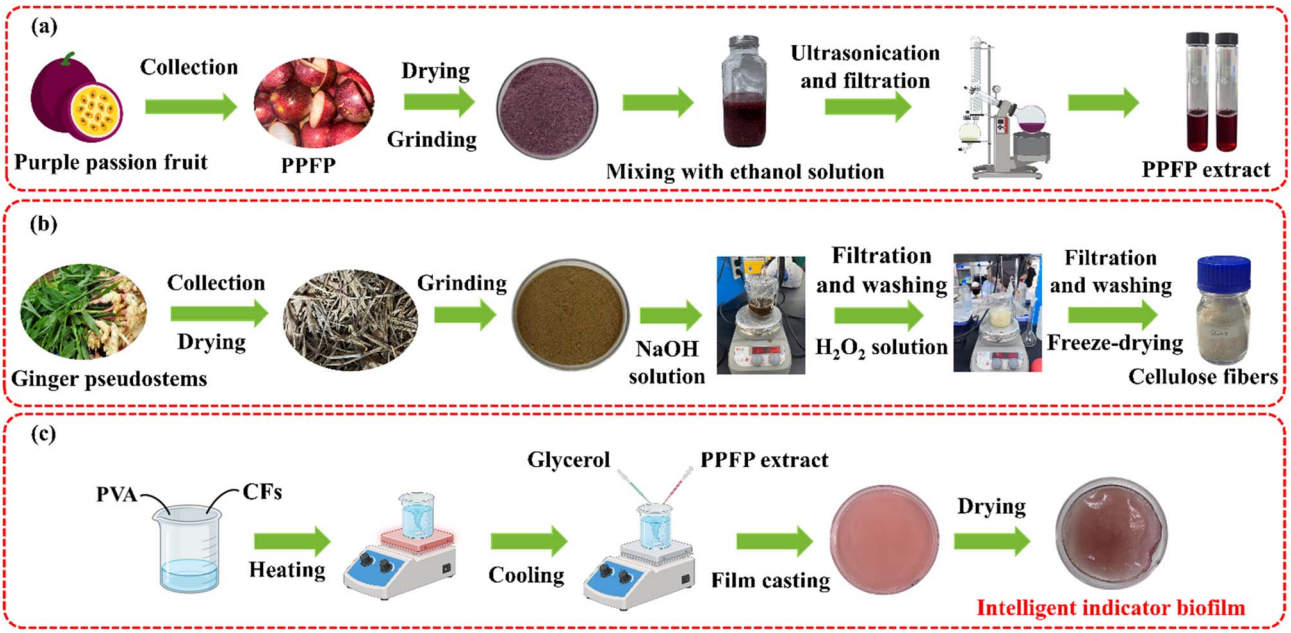

Fig. 1 Schematic representation of (a) anthocyanin extraction from purple passion fruit peel, (b) cellulose fiber extraction from ginger pseudostem, and (c) the film preparation process.

decreased to below 40 °C, 30 wt% glycerol was added as a plasticizer and stirring was continued until a homogeneous solution was obtained. The PPFP extract was subsequently incorporated into the mixture at a concentration of 25% (v/v), followed by gentle stirring for 15–30 min. The resulting solution was ultrasonicated to remove entrapped air bubbles, cast by pouring 30 mL of the mixture into Petri dishes with a diameter of 140 mm, and dried at 40 °C for 24 h. To evaluate the effects of anthocyanin incorporation and cellulose fibers concentration on the properties of the resulting films, the anthocyanin content was fixed, while the CFs content was varied at 0.5 wt%, 1.0 wt%, and 1.5 wt% relative to the used PVA mass. The samples consisting of neat PVA, PVA with anthocyanin, and PVA with anthocyanin reinforced with different CFs contents were denoted as PVA, PA, PA-0.5, PA-1.0, and PA-1.5, respectively. The film fabrication process and compositions were presented in Fig. 1c and Table 1, respectively.

2.3. Characterization analysis

2.3.1. Anthocyanin content of PPFP extract. The anthocyanin content of the extract was determined using the pH differential method by quantifying monomeric anthocyanins *via* UV-Vis spectrophotometry, following the method described by Giusti and Wrolstad.[16] The extract was diluted with 0.025 M potassium chloride (KCl) buffer at pH 1.0 and 0.4 M sodium acetate (CH_3COONa) buffer at pH 4.5. The absorbance of the samples at pH 1.0 and pH 4.5 was measured at wavelengths of 520 nm and 700 nm using appropriate dilution factors until the absorbance at 520 nm fell within the linear range of the spectrophotometer (<1.2). The solutions were allowed to equilibrate for 15 min prior to measurement. The total anthocyanin content (TAC) of the extract was expressed as cyanidin-3-glucoside (Cy-3-glc) and calculated as follows:

$$A = (A_{520} - A_{700})_{\mathrm{pH}_{1.0}} - (A_{520} - A_{700})_{\mathrm{pH}_{4.5}} \quad (1)$$

$$\mathrm{TAC}(\mathrm{mg\ g^{-1}}) = \frac{A \times M_W \times \mathrm{DF} \times 10^3}{\varepsilon \times l} \times \frac{V_s}{m} \quad (2)$$

where A = absorbance, TAC = total anthocyanin content, M_W = molecular weight of cyanidin-3-glucoside (449.2 g mol^{-1}), DF = dilution factor (ratio between total volume and volume of aliquot added to buffer), ε = molar absorptivity of cyanidin-3-glucoside (26 900 L × mol^{-1} × cm^{-1}), l = pavelength (cm), V_s = solvent volume (L), m = mass of the raw material (g).

2.3.2. UV-vis spectra measurement of PPFP extract at different pH values. The UV-Vis absorption spectra of the PPFP extract were recorded at different pH values (1–14) over the wavelength range of 450–700 nm using a UV-Vis spectrophotometer (JASCO V-730, Japan) to investigate the color changes of the extract in response to pH variations. The pH of the buffer solutions was adjusted using HCl or NaOH solutions.

2.3.3. Anthocyanin degradation kinetics. The effect of storage temperature on anthocyanin stability was evaluated using a first-order reaction kinetics model. The anthocyanin extract was stored in amber glass vials under dark conditions at

Table 1 The weight percentage and volume percentage compositions of the fabricated smart films

Sample	PVA (%, wt/v)	CFs content (wt%)	Glycerol (wt%)	PPFP extract (%, v/v)
PVA	5	0	30	25
PA	5	0	30	25
PA-0.5	5	0.5	30	25
PA-1.0	5	1.0	30	25
PA-1.5	5	1.5	30	25

two temperatures, 4 °C and room temperature, for 8 days. The anthocyanin content was determined at two-day intervals. The kinetic rate constant (k) of thermal degradation was determined by regression analysis of experimental data based on the initial anthocyanin content as a function of increasing time, as described by the following eqn (3):[17]

$$\ln\left(\frac{C_t}{C_0}\right) = -k \times t \tag{3}$$

where C_t is the anthocyanin content (mg g^{-1}) at time t, C_0 is the initial anthocyanin content (mg g^{-1}), k is the rate constant (day^{-1}), and t is the time (days).

The half-life ($t_{1/2}$) of the degradation process is described by eqn (4):[17]

$$t_{1/2}(\text{day}) = \frac{\ln(2)}{k} \tag{4}$$

where k is the kinetic rate constant (day^{-1}).

2.3.4. Colour measurement. The color of the cellulose samples was determined using a CS-10 Portable 8 mm Colorimeter. The CIE L^*, a^*, and b^* color parameters were recorded, and the total color difference (ΔE) between the cellulose samples and the standard white reference was calculated using eqn (5) and (6).[18]

$$\Delta E = \sqrt{\Delta L^{*2} + \Delta a^{*2} + \Delta b^{*2}} \tag{5}$$

$$\Delta L = L_1^* - L_0^*,\ \ \Delta a = a_1^* - a_0^*,\ \ \Delta b = b_1^* - b_0^* \tag{6}$$

where L_1^*, a_1^*, and b_1^* denote the lightness, red–green, and yellow–blue chromaticity coordinates of the cellulose samples, respectively, and L_0^*, a_0^*, and b_0^* correspond to those of the standard white reference. The L^*, a^*, and b^* parameters were defined according to the CIE Lab color space. The whiteness index (WI) of the cellulose samples and the standard white reference were calculated using eqn (7).[19]

$$\text{WI} = 100 - \sqrt{(100 - L^*)^2 + a^{*2} + b^{*2}} \tag{7}$$

2.3.5. Fourier transform infrared (FTIR) spectroscopy. The FTIR spectra of the cellulose fibers and film samples were analyzed using an FTIR spectrometer (Nicolet 6700, Thermo Scientific). The spectra were measured over the wavenumber range of 4000–500 cm^{-1} with 32 scans at a resolution of 4 cm^{-1}.

2.3.6. X-ray diffraction (XRD). X-ray diffraction (XRD) analysis was performed to investigate the crystalline structure of the cellulose fibers and film samples using an EMPYREAN diffractometer (PANalytical, The Netherlands). Measurements were conducted over a diffraction angle range of 5–60° (2θ) using Cu Kα radiation (λ = 1.54056 Å), operated at an accelerating voltage of 40 kV and a current of 45 mA. The crystallinity index (CrI) was calculated by the method of Segal *et al.*[20]

$$\text{CrI}(\%) = \frac{(I_{200} - I_{\text{am}})}{I_{200}} \times 100 \tag{8}$$

where I_{200} represents the maximum intensity of the diffraction peak corresponding to the (200) crystalline plane, and I_{am} denotes the diffraction intensity of the amorphous region. For cellulose, the (200) diffraction peak appears at approximately 2θ = 22°, while the amorphous contribution corresponds to the minimum intensity at around 2θ = 18°. For PVA films, the diffraction peak of the (101) plane is observed at approximately 2θ = 19°, and the amorphous intensity is taken at around 2θ = 16°.[21]

2.3.7. Field-emission scanning electron microscopy (FE-SEM). The morphology of the cellulose and film samples was characterized by field-emission scanning electron microscopy (FE-SEM, S-4800, Hitachi). The observations were performed at an accelerating voltage of 10 kV over a magnification range of 200×–2000×. Before imaging, the samples were affixed to metal stubs and sputter-coated with a thin platinum (Pt) layer to enhance surface conductivity.

2.3.8. Thermogravimetric analysis (TGA). The thermal stability of the cellulose fibers was evaluated using a thermogravimetric analyzer (STA PT 1600, Linseis, Germany). Thermogravimetric analysis (TGA) was conducted at a heating rate of 10 °C min^{-1} from 25 to 600 °C under an argon atmosphere. The mass loss associated with thermal degradation was continuously recorded as a function of temperature. In addition, the derivative thermogravimetric (DTG) curves were obtained to determine the temperature corresponding to the maximum rate of mass loss.

2.3.9. Thickness and moisture content. The film thickness was measured using a digital thickness gauge (Mitutoyo 547-401A) with an accuracy of 3 μm. The thickness was measured at three random positions on each film. The moisture content of the film samples was determined using a gravimetric method. The film samples were cut into 2 × 2 cm pieces and then dried in an oven at 105 °C until a constant weight was reached. The moisture content of the film samples was calculated according to the following eqn (9):[22]

$$\text{Moisture content}(\%) = \frac{m_1 - m_2}{m_1} \times 100 \tag{9}$$

where m_1 and m_2 are the weights of the film before and after drying (g), respectively.

2.3.10. Water vapor permeability. The water vapor permeability (WVP) of the film samples was determined according to the method reported by Zhengang Xie *et al.*,[23] with slight modifications. First, 3 g of $CaCl_2$ was added to a glass vial, which was then sealed with the film samples. Subsequently, the vials were placed in a desiccator at a relative humidity of 75% and 25 °C for 24 h. The WVP value was calculated using the following eqn (10):[22]

$$\text{WVP}\left(\text{g m}^{-1}\ \text{s}^{-1}\ \text{Pa}^{-1}\right) = \frac{\Delta m \times d}{t \times S \times P} \tag{10}$$

where Δm is the mass of water vapor transmitted through the film (g), d is the film thickness (mm), t is the time (s), S is the effective permeation area of the film (m^2), and P is the vapor pressure of a saturated NaCl solution (1753.55 Pa).

2.3.11. Water solubility. The water solubility (WS) of the film samples was determined according to the method reported by Kailong Zhang *et al.*,[24] with minor modifications. First, the

film samples were dried at 50 °C to constant weight. Subsequently, the samples were immersed in 50 mL of distilled water at room temperature and stirred continuously for 1 h. After that, the films were filtered and dried again at 50 °C to constant weight.

$$\mathrm{WS}(\%) = \frac{m_0 - m_1}{m_0} \times 100 \quad (11)$$

where m_0 and m_1 are the dry weights of the films before and after immersion in distilled water, respectively (g).

2.3.12. Mechanical properties. The mechanical properties, including tensile strength (MPa), elongation at break (%), and Young's modulus (MPa), were determined using a universal testing machine (AGS-X, Shimadzu, Japan) in accordance with a modified ASTM D882 standard. The initial gauge length and crosshead speed were set to 50 mm and 10 mm min^{-1}, respectively. Three replicates were prepared for each film. The obtained films were then conditioned at 23 ± 2 °C and 50 ± 10% relative humidity for 48 h prior to mechanical testing.

2.3.13. The pH-sensitive property of films. The pH-sensitive property of film was measured according to the method of Jiang *et al.*[25] Film sample (2 cm × 2 cm) was immersed in different buffer solutions ranging from pH 2 to 12.

2.3.14. Application in food freshness detection. In this study, the prepared films were applied as freshness indicators for monitoring the quality of fresh shrimp. Film samples with dimensions of 2 × 2 cm were fixed to the inner surface of trays containing 50 g of shrimp. The trays were tightly sealed with plastic wrap and stored at 4 °C.[26] The freshness evaluation was carried out at 12 h intervals.

2.3.15. Statistical analysis. Analysis of variance (ANOVA) and Tukey's test were performed using IBM SPSS Statistics 20 for Windows. All experiments were conducted in triplicate (n = 3) and analyzed by one-way ANOVA at a 95% confidence level, with p-values lower than 0.05 indicating statistically significant differences.

3. Results and discussion

3.1. Characterization of PPFP extract

3.1.1. Effect of solvent concentration on total anthocyanin content. Fig. 2 illustrated the influence of ethanol concentration on the total anthocyanin content extracted from purple passion fruit peel. The polarity of the solvent played a crucial role in the efficiency of anthocyanin extraction.[27] The polarity balance between ethanol and water in the solvent mixture created favourable conditions for extracting soluble compounds at appropriate ratios.[28] Therefore, ethanol concentrations of 20%, 40%, 60%, and 80% were used for anthocyanin extraction.

As shown in Fig. 2, when the ethanol concentration increased from 20% to 40%, the anthocyanin content gradually increased from 1.01 to 1.25 mg cyanidin 3-*O*-glucoside equivalents (C3G)/g dry weight (DW). The highest anthocyanin yield was obtained at 60% ethanol, reaching 1.53 mg C3G per g DW. However, when the ethanol concentration increased to 80%, the anthocyanin content decreased to 1.36 mg C3G per g DW, indicating a notable decline compared with the 60% level. This

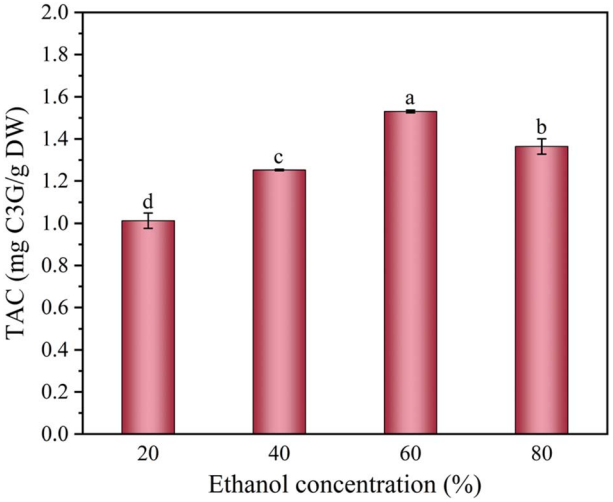

Fig. 2 Effect of ethanol concentration on total anthocyanin content.

decrease was explained by the chemical nature of anthocyanins. As polar polycyclic aromatic organic compounds containing multiple hydroxyl groups, anthocyanins dissolved well in polar organic solvents,[29] and their solubility strongly depended on the polarity of the solvent system.[30] In this study, aqueous ethanol was used as the extraction solvent. The relative polarity of water (1.0) was higher than that of ethanol (0.654).[31] Therefore, when the ethanol concentration became too high, the reduction in water content lowered the overall polarity of the solvent system, which reduced the solubility of anthocyanins present in purple passion fruit peel.[32] Consequently, the extracted anthocyanin yield decreased.

These results indicated that 60% ethanol was the most suitable solvent concentration for extracting anthocyanins from purple passion fruit peel. This finding was consistent with the study by Zhou *et al.*,[33] who reported that increasing ethanol concentration from 50% to 70% significantly enhanced anthocyanin extraction from grape pomace; however, further increases from 70% to 90% did not lead to substantial improvement in extraction efficiency. Furthermore, the ANOVA results indicated that variations in ethanol concentration from 20 to 80% had a statistically significant effect on the total anthocyanin content ($p < 0.05$), as presented in Table S4 of the Supplementary Information.

3.1.2. Effect of the material-to-solvent ratio on total anthocyanin content. The influence of the material-to-solvent ratio on anthocyanin extraction efficiency was illustrated in Fig. 3. The ratios evaluated in the extraction process included 1 : 15, 1 : 20, and 1 : 25 (wt/v). At these ratios, the anthocyanin content showed an increasing trend, with values of 1.46 mg C3G per g DW, 1.44 mg C3G per g DW, and 1.53 mg C3G per g DW, respectively. This increase was attributed to the increase in the material-to-liquid ratio, which enhanced the contact between the raw material and the solvent, thereby increasing the extracted anthocyanin content in the extract.[34] Moreover, the transport of solutes from inside plant cells to the surrounding solvent occurred primarily through diffusion, which further improved the extraction rate and efficiency.[35] However, when

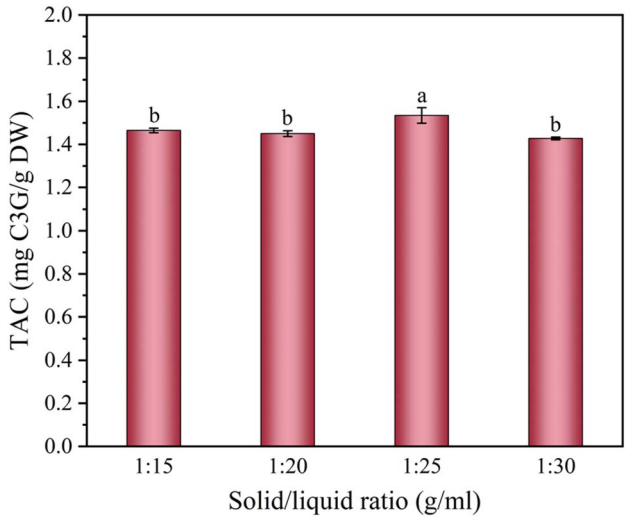

Fig. 3 Effect of the material-to-solvent ratio on total anthocyanin content.

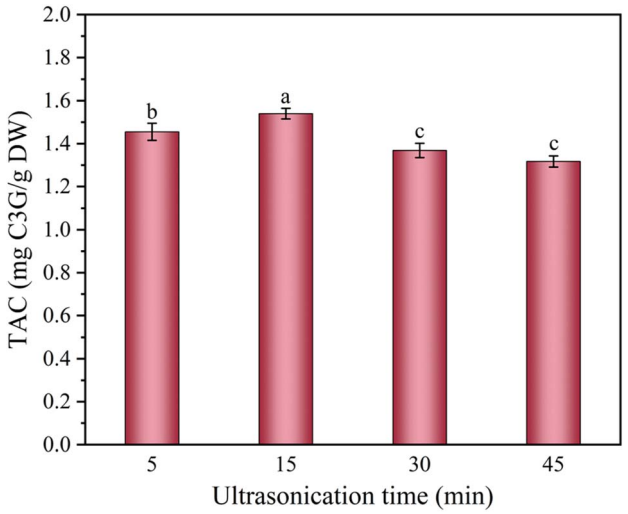

Fig. 4 Effect of ultrasound time on total anthocyanin content.

the material-to-solvent ratio was further increased to 1 : 30 (wt/v), the anthocyanin content decreased to 1.43 mg C3G per g DW. Although a higher solvent volume generally promoted the diffusion of anthocyanins into the extraction medium, once the system reached equilibrium, further increases in solvent volume did not improve anthocyanin extraction efficiency.[35] Moreover, excessive solvent volume could reduce the anthocyanin content in the extract, as a portion of anthocyanins was oxidized during the extraction process.[34] The findings indicated that a ratio of 1 : 25 (w/v) was the most suitable for subsequent experiments in this study. Furthermore, ANOVA analysis demonstrated that variations in the material-to-solvent ratio had a statistically significant effect on the total anthocyanin content ($p < 0.05$), as presented in Table S5 of the Supplementary Information. The influence of the material-to-solvent ratio on anthocyanin extraction from purple passion fruit peel under UAE conditions was similar to the results reported by Tuan *et al.*,[36] who demonstrated that extraction efficiency increased markedly from 68% to 94.4% when the ratio varied from 1 : 15 to 1 : 25 (w/v).

3.1.3. Effect of ultrasound time on total anthocyanin content. Ultrasound time played an essential role in the extraction process.[37–39] The effect of ultrasound duration on total anthocyanin content was shown in Fig. 4. When the ultrasound time increased from 5 to 15 minutes, the extraction yield increased significantly, with the anthocyanin content rising from 1.19 mg C3G per g DW to 1.53 mg C3G per g DW. However, further extending the ultrasound time to 30 and 45 minutes caused a notable decrease in anthocyanin content, with recorded values of 1.36 mg C3G per g DW and 1.31 mg C3G per g DW, respectively. This decline could be attributed to prolonged exposure to ultrasonic waves, which generated heat and high pressure that potentially altered or degraded anthocyanins.[40] Therefore, the optimal extraction time in this study was determined to be 15 minutes, which ensured high extraction efficiency while minimizing anthocyanin degradation. In addition, ANOVA analysis demonstrated that variations in ultrasound treatment time had a statistically significant effect on the total anthocyanin content ($p < 0.05$), as presented in Table S6 of the Supplementary Information. This finding further highlighted the advantage of UAE, which provided rapid extraction compared with conventional techniques. Similarly, Tuan *et al.*,[36] reported that ultrasound-assisted extraction of anthocyanins from purple passion fruit peel at 5–20 minutes yielded the highest extraction efficiency (80.94%) after 10 minutes, while prolonged sonication up to 20 minutes led to anthocyanin degradation due to temperature, oxygen, and light exposure.

Based on the analyses of ethanol concentration, material-to-solvent ratio, and ultrasound duration, the optimal conditions for ultrasound-assisted extraction of anthocyanins from purple passion fruit peel were identified. The extraction solvent was 60% acidified ethanol, the material-to-solvent ratio was 1 : 25, and the extraction time was 15 minutes. In addition, other parameters were controlled, including extraction temperature (35–40 °C). These results confirmed that ethanol concentration, material-to-solvent ratio, and ultrasound time significantly affected the total anthocyanin content obtained from purple passion fruit peel.

In this study, the anthocyanin content extracted from freeze-dried PPFP using ultrasound-assisted extraction (UAE) was significantly higher than that obtained from hot-air-dried PPFP reported by Sakulrang *et al.*[9] However, it remained lower than that of anthocyanin-rich materials, as shown in Table 2. These variations could be attributed to differences in anthocyanin composition among plant species and plant parts.[41] In addition, raw material quality, processing methods, and storage conditions also played essential roles, alongside the selection of appropriate solvents and extraction parameters.[42]

3.1.4. pH-responsive color change and UV-vis spectral characteristics of PPFP extract. The stability of the PPFP extract was influenced by pH, and the results showed noticeable and diverse color changes under different pH conditions. The color

Table 2 Comparison of anthocyanin content extracted in this study with values reported for other raw materials

No.	Source	Extraction method	Total anthocyanin content	References
1	Purple passion fruit peels	Ultrasound-assisted extraction	1.539 mg g^{-1}	This study
2	Purple passion fruit peels (hot-air-dried)	Ultrasound-assisted extraction	0.28 mg g^{-1}	9
3	Purple sweet potatoes	Ultrasound-assisted extraction	214.92 mg/100g	43
4	Pomegranate peels	Ultrasound-assisted extraction	0.35 mg g^{-1}	44
5	Mangosteen peels	Ultrasound-microwave assisted extraction	108 mg/100g	45
6	Black rice	Solvent extraction method	116.58 mg/100g	46
7	Hibiscus	Solvent extraction method	359.3 mg/100g	47
8	Blackberry	Ultrasound-assisted deep eutectic solvent extraction	193.03 mg/100 g	48
9	Grape skins	Ultrasound-assisted enzymatic extraction	3.01 mg g^{-1}	49
10	Black soybeans	Solvent extraction method	136.68 mg/100g	50

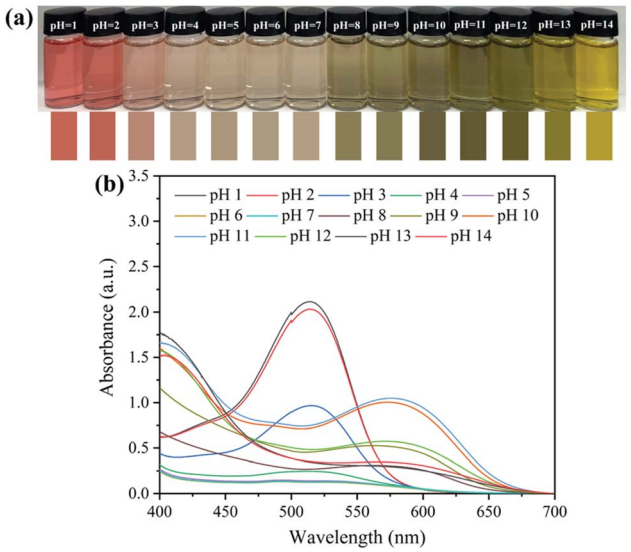

Fig. 5 (a) Color changes of PPFP extract at pH 1–14; (b) UV-Vis spectra of PPFP extract at pH 1–14.

shifted from red, pink, colorless, green, to yellow, corresponding to solutions ranging from acidic to alkaline, as shown in Fig. 5a. Anthocyanins are relatively more stable in acidic environments than in neutral or alkaline conditions.[51] In buffer solutions with pH values from 1 to 14, the PPFP extract appeared red-pink at pH 1–2 and changed to light pink at pH 3. The color gradually faded and became colorless at pH 4–7. Under alkaline conditions, the color changed again, turning increasingly green at pH 8–11 and transitioning from green to yellow at pH 12–14. This phenomenon could be explained by the coexistence of different anthocyanin structural forms at different pH levels. The structure shifted from flavylium cation (red) at pH 1–3 to carbinol pseudobase (colorless) at pH 4–7, to the anionic quinonoidal base (green) at pH 8–11, followed by the formation of chalcones (yellow) at pH 12–14. The color-change mechanism of anthocyanins at different pH values was presented in Fig. 6. Similar color transitions were also observed in purple passion fruit peel extracts reported by Jiang *et al.*[52]

The influence of pH on color stability was further evaluated by measuring the absorbance of the extracts using a UV-Vis spectrophotometer. The color variations at pH 1–14 corresponded to changes in absorbance at characteristic wavelengths, as shown in Fig. 5b. A maximum absorption peak was observed at approximately 512 nm at pH 1–4, and the absorbance gradually decreased as pH increased. The absorption peak shifted from 512 nm to approximately 570 nm, with the absorbance increasing as pH increased from 8 to 11 and

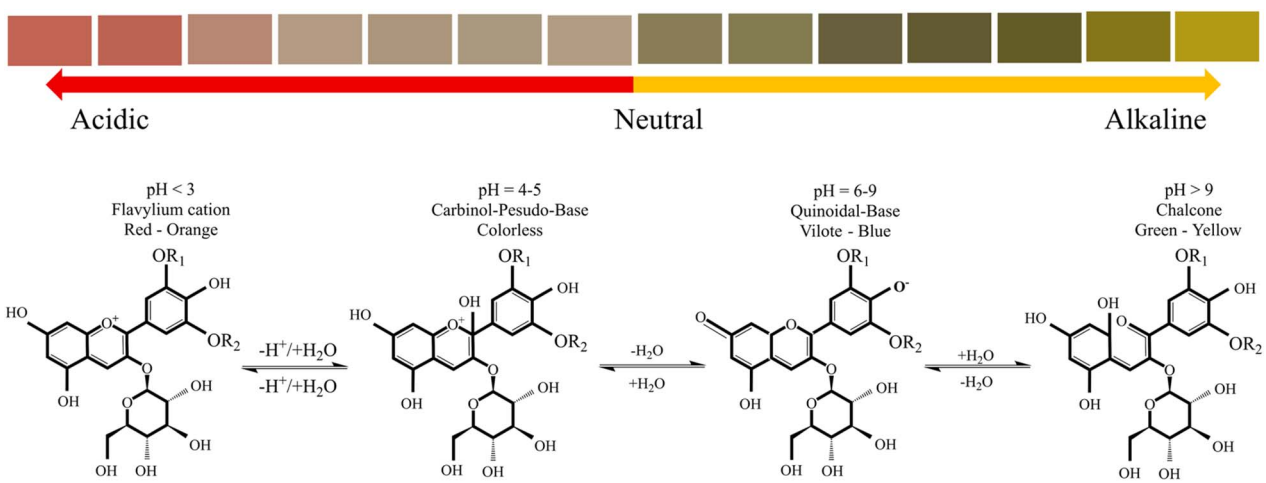

Fig. 6 The color-change mechanism of anthocyanins at different pH values.

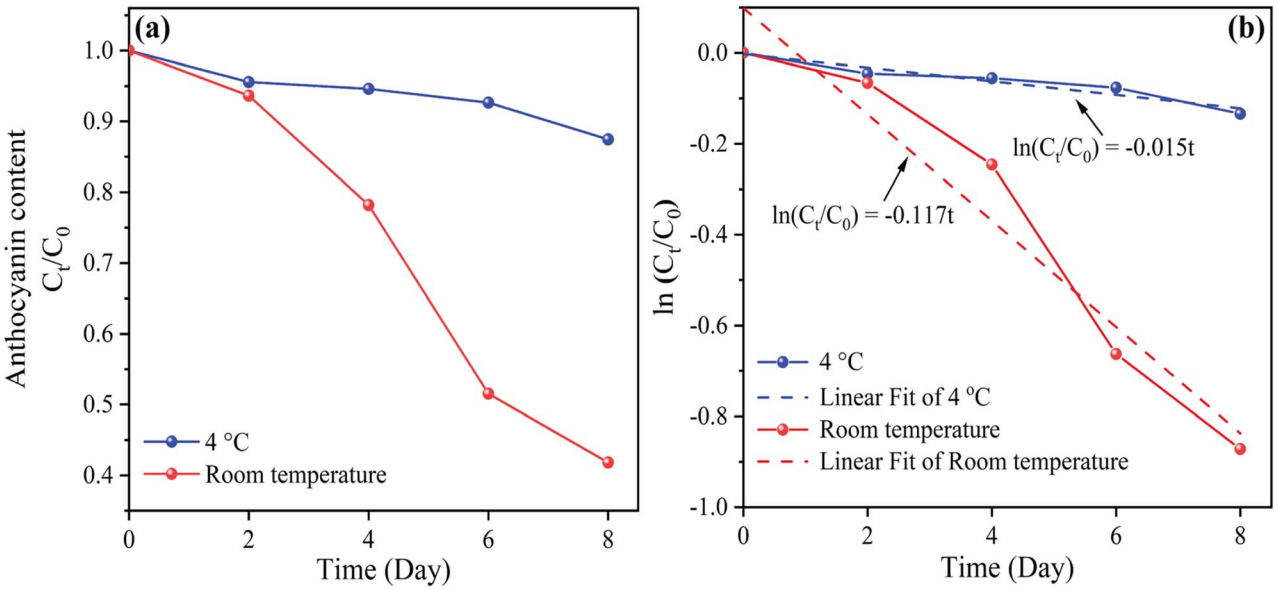

Fig. 7 (a) Reduction in anthocyanin content and (b) degradation kinetics of anthocyanins as a function of time at two different storage temperatures.

decreasing again when pH increased from 12 to 14. These spectral changes reflected the structural transformations caused by the shift from acidic to alkaline conditions and corresponded well with the color changes shown in Fig. 5a. Similar peak shifts were also recently reported by Jiang *et al.*[52] Overall, the PPFP extract exhibited pronounced pH-responsive color changes, indicating strong potential for applications in intelligent colorimetric indicator films.

3.1.5. Effect of temperature on total anthocyanins content. The effect of temperature on the degradation of anthocyanins extracted from purple passion fruit peel was investigated under two different storage conditions, namely 4 °C (refrigeration) and room temperature, as presented in Fig. 7a. The thermal degradation kinetics of anthocyanins at these two storage temperatures followed a first-order reaction model, as evidenced by the linear relationship between the logarithm of the concentration ratio (C_t/C_0) and time,[53] with regression coefficients in the range of $0.935 < R^2 < 0.941$, as shown in Table 3.

In addition, the degradation rate of anthocyanins increased with storage temperature, as shown in Fig. 7b. The results showed that the degradation rate constant (k) of the sample stored at room temperature (0.117 day^{-1}) was higher than that at 4 °C (0.015 day^{-1}). This result demonstrated that an increase in storage temperature accelerated the degradation rate of anthocyanins.[17] Furthermore, the half-life ($t_{1/2}$) at 4 °C was 7.8 times higher than that of the sample stored at room temperature. These results were consistent with a previous study on *Hibiscus sabdariffa* reported by André Sinela *et al.*,[54] which showed that when the storage temperature increased from 4 °C to 37 °C, the k values increased from 0.24×10^{-7} (s^{-1}) to 9.2×10^{-7} (s^{-1}). In addition, a study by Suwalee Fong-in *et al.*[55] showed that the half-life ($t_{1/2}$) of anthocyanins extracted from Riceberry rice flour decreased from 210 min to 103.2 min as the temperature increased from 70 to 100 °C.

These results demonstrated that anthocyanins extracted from purple passion peel tended to degrade more rapidly with increasing storage temperature, which was consistent with their thermally sensitive nature.

Table 3 Kinetic parameters of anthocyanin degradation

Sample	R^2	k (day^{-1})	$t_{1/2}$ (day)
4 °C	0.935	0.015	46.210
Room temperature	0.941	0.117	5.924

3.2. Characterization of cellulose fibers extracted from ginger pseudostems

3.2.1. Color analysis. The color parameters presented in Table 4 indicate that the chemical treatment had a significant effect on the color characteristics of the extracted cellulose fibers. Compared with the ginger stem raw material, the cellulose samples exhibited higher L* and WI values and lower ΔE values, approaching those of the standard white reference. This suggests that the applied chemical treatments effectively remove non-cellulosic components, such as lignin, hemicellulose, and colored extractives, which are primarily responsible for the yellowish appearance of the raw material. Furthermore, a noticeable decrease in the b* values was observed for the cellulose samples, indicating a reduction in yellowness. This trend can be attributed to the degradation and removal of chromophoric groups associated with lignin during alkaline treatment and peroxide bleaching. The oxidative action of H_2O_2 under alkaline conditions disrupts conjugated aromatic structures, thereby reducing yellowing and improving the whiteness of the extracted cellulose fibers. A similar enhancement in cellulose whiteness has been reported by

Table 4 Color parameters (L, a^*, b^*), total color difference (ΔE), and whiteness index (WI) of ginger pseudostem and extracted cellulose fibers

Sample	L*	a*	b*	ΔE	WI	Photo
GP	23.84	−0.01	15.55	77.98	22.27	
CFs	76.50	3.87	23.98	39.50	66.20	
Standard	97.66	3.13	−9.37	0.00	89.85	—

Fitriana *et al.*[56] following alkaline pretreatment and H_2O_2 bleaching of sugar palm fibers, corroborating the effectiveness of this chemical treatment strategy.

3.2.2. Fourier transform infrared spectroscopy (FTIR) analysis. The chemical composition of the ginger stem sample and the chemically treated extracted cellulose fibers were investigated by Fourier transform infrared spectroscopy, as shown in Fig. 8. The main constituents of plant fibers were cellulose, hemicellulose, and lignin.[57] The FTIR spectra revealed a broad absorption band in the range of 3700–3000 cm^{-1} with a maximum peak at 3421 cm^{-1}, which was attributed to the stretching vibration of O–H bonds and was observed in all samples. The absorption band at 2908 cm^{-1}, which was present in all samples, corresponded to the stretching vibration of C–H bonds associated with alkyl groups in the chemical structure of cellulose.[58] The peak at 1740 cm^{-1} observed in the GP sample was assigned to the C=O stretching vibration characteristic of acetyl and uronic ester groups in pectin or hemicellulose, as well as ester linkages of carboxylic groups in lignin (ferulic and *p*-coumaric acids forming ester bonds) and hemicellulose.[59]

Furthermore, the band at 1637 cm^{-1} detected in all samples was attributed to the bending vibration of O–H bonds associated with absorbed water.[60] Additional absorption bands at 1510 cm^{-1} and 1240 cm^{-1} were related to C=C vibrations of aromatic rings present in lignin[58] and C–O stretching vibrations characteristic of aryl groups in lignin, respectively.[59] The band at 1375 cm^{-1} corresponded to the bending vibration of C–H bonds in the chemical structure of cellulose and hemicellulose.[61] Finally, the absorption band at 1060 cm^{-1} was attributed to the C–O–C stretching vibration of the pyranose ring in cellulose,[62] while the band at 897 cm^{-1} was associated with glycosidic C–H deformation, along with ring vibration and O–H bending, which were characteristic of β-glycosidic linkages between anhydroglucose units in the cellulose structure.[59]

Compared with the FTIR spectrum of the ginger pseudostem sample, the spectra of the extracted cellulose fibers exhibited a marked reduction in the intensities of the absorption bands at 1740 cm^{-1}, 1510 cm^{-1}, and 1240 cm^{-1}. This observation indicated that the chemical treatment effectively removed hemicellulose and lignin from the raw material. In addition, the increased intensity of the absorption band at 897 cm^{-1} further confirms the efficient elimination of non-cellulosic components and the enhanced purity of the extracted cellulose fibers.

3.2.3. X-ray diffraction (XRD) analysis. Fig. 9 presented the X-ray diffraction (XRD) patterns and crystallinity index of the ginger pseudostem sample and the extracted cellulose fibers. The characteristic diffraction peaks were observed at $2\theta = 15°$, 15.9°, 22.2°, and 34.6°, corresponding to the $(1\bar{1}0)$, (110), (200), and (004) lattice planes, respectively, which were characteristic of the crystalline structure of cellulose I.[62] The crystallinity index of the ginger pseudostem and the extracted cellulose fibers were 28.39% and 74.65%, respectively. These results indicated that the pretreatment and bleaching processes effectively removed non-cellulosic components, thereby significantly increasing the crystallinity of the extracted cellulose.[63] Furthermore, the crystallinity index of the extracted cellulose fibers was higher than

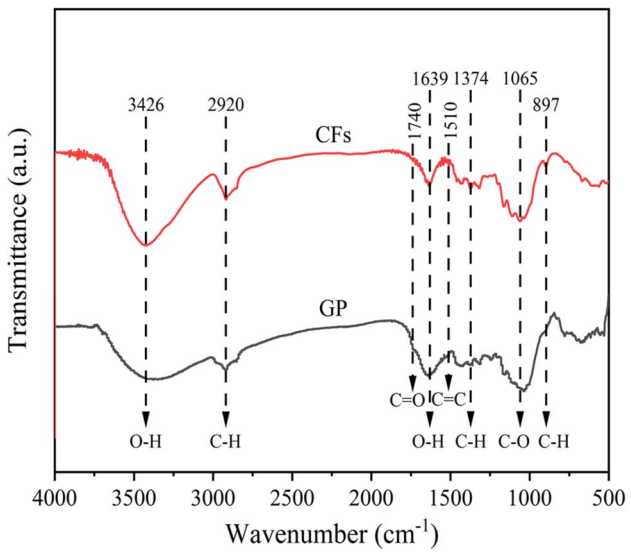

Fig. 8 FTIR spectra of the ginger pseudostem (GP) and cellulose fibers (CFs).

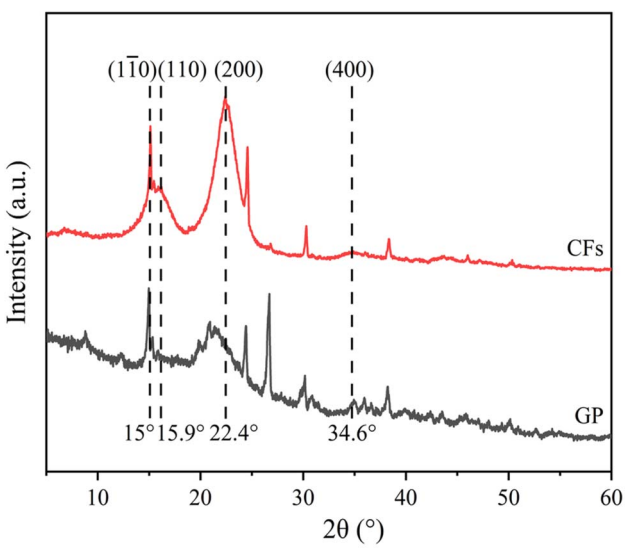

Fig. 9 XRD patterns of ginger pseudostem (GP) and cellulose fibers (CFs).

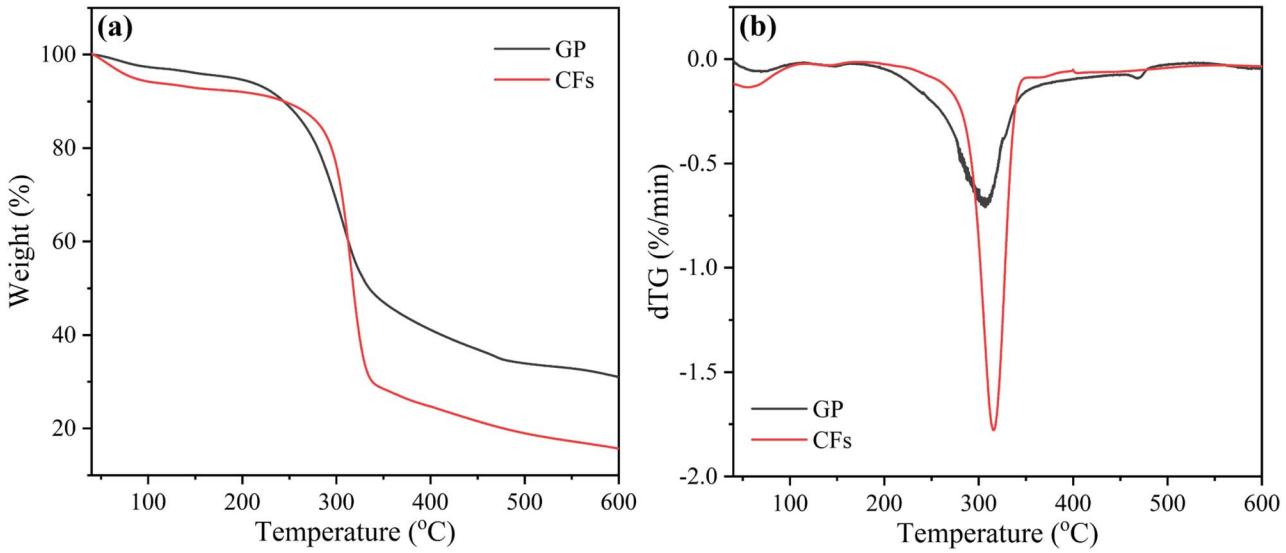

Fig. 10 TGA (a) and DTG (b) curves of ginger pseudostem (GP) and cellulose fibers (CFs).

those reported in previous studies, including 71.8% reported by Zendrato *et al.*[64] and 67% reported by Zaki *et al.*[65]

3.2.4. Thermogravimetric analysis (TGA). The TGA and DTG curves of the ginger pseudostem sample and the cellulose fibers were presented in Fig. 10. The thermal degradation of the samples showed three main stages of mass loss: stage (I) occurred below 125 °C, stage (II) occurred in the range of 125–370 °C, and stage (III) occurred from 370 to 600 °C. In stage I, which occurred from 40 to 125 °C, both samples exhibited a small mass loss of approximately 4% and 7% for the ginger pseudostem and cellulose fibers, respectively. The mass loss in this stage was attributed to the removal of moisture, water, and low-molecular-weight components.[58] Stage II was the main degradation stage, showing significant mass loss within the temperature range of 125–370 °C. The initial degradation temperatures of the ginger pseudostem and cellulose fibers were approximately 210 °C and 235 °C, respectively, with mass losses of 52.43% for the ginger pseudostem and 66.86% for the extracted cellulose fibers. The thermal degradation of hemicellulose and cellulose occurred at around 260 °C and 375 °C, respectively, while the degradation of lignin occurred over a broad range of 250–450 °C.[59]

Fig. 10 showed that the obtained cellulose fibers exhibited higher thermal stability than the ginger pseudostem. This could be explained by the fact that the chemical treatment effectively removed hemicellulose and lignin from the chemical structure of the ginger pseudostem. The final degradation stage was the carbonization stage, which occurred within the temperature range of 370–600 °C, with the residual mass being 31% for the ginger pseudostem and 15.66% for the cellulose fibers. These results indicated that the chemical treatment effectively removed components such as hemicellulose, lignin, and other non-cellulosic substances from the ginger pseudostem structure, resulting in cellulose fibers with improved thermal stability.

3.2.5. Scanning electron microscope (SEM) analysis. The surface morphology of the ginger pseudostem sample and cellulose fibers was observed through SEM images, as illustrated in Fig. 11. The SEM images of the obtained cellulose fibers showed significant changes compared to the raw material. Fig. 11a and b showed that the ginger pseudostem had a rough and irregular surface, and the cellulose fibrils tended to aggregate and form fiber bundles. In addition, the ginger pseudostem exhibited sheet-like structures and clusters of sharp-edged features. This was believed to be due to the presence of components such as lignin, hemicellulose, and other non-cellulosic substances, which acted as binding agents for the cellulose fibrils. For the extracted cellulose fibers, significant changes in the surface structure of the ginger pseudostem were observed, as shown in Fig. 11c and d. The cellulose fibers obtained from the ginger pseudostem exhibited distinct fibrous structures with smooth and uniform surfaces. This notable change in surface morphology resulted from the chemical treatment, which effectively removed lignin, hemicellulose, and other non-cellulosic components. This result was consistent with the findings reported by Zendrato *et al.*[64] In addition, dynamic light scattering (DLS) results indicated that the obtained cellulose fibers exhibiting an average diameter of approximately 420 nm (0.42 μm), as shown in Fig. S1 of the SI.

3.3. Characterization of films

3.3.1. Thickness and moisture content. The thickness and moisture content of the film samples were presented in Fig. 12. The incorporation of anthocyanin and cellulose fibers increased the thickness of the PVA-based films, with values ranging from 0.099 to 0.160 mm, as shown in Fig. 12a. This phenomenon can be attributed to the presence of cellulose fibers and anthocyanin, which formed a more complex network structure compared to the neat PVA film, thereby leading to an increase in film thickness.[47] This result is consistent with the study by Zhenkun Xiao *et al.*,[66] which reported that film thickness increased when curcumin was incorporated at concentrations of 0.5–4.5% into the PVA/CS matrix.

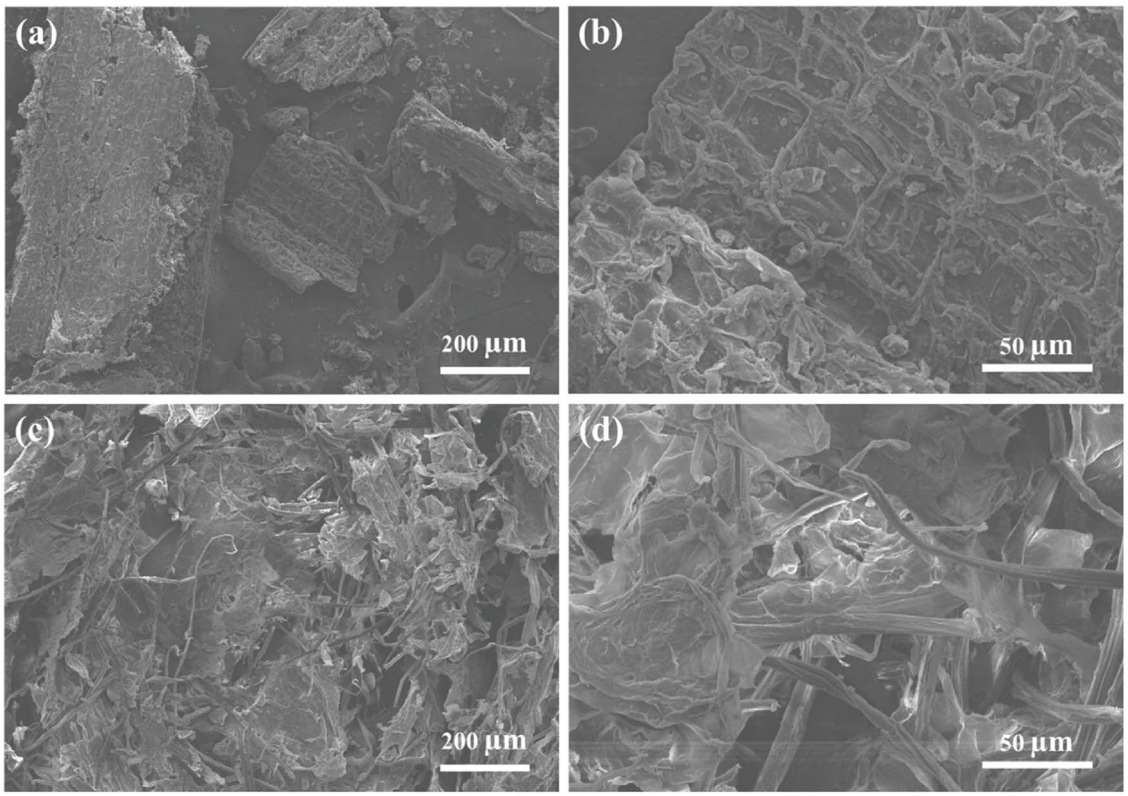

Fig. 11 SEM images of samples: (a, b) Ginger pseudostem; (c, d) Cellulose fibers.

In addition, moisture content is an important factor affecting the applicability of films in food preservation. The moisture content of the obtained films showed a decreasing trend from 39.19% to 13.22%, as illustrated in Fig. 12b. This finding is similar to that reported by Cyrine Amara *et al.*,[67] where the incorporation of cellulose microfibers at concentrations of 1–10% resulted in a reduction in film moisture content.

3.3.2. Water solubility. The water solubility of the film samples is presented in Fig. 13. The results showed that the neat PVA film exhibited a water solubility of 36.13 ± 6.85%, which was lower than that of the PA sample (41.23 ± 4.90%). This difference could be attributed to the dissolution of anthocyanin molecules during immersion in water, which increased the solubility of PVA films upon anthocyanin incorporation.[68] A study by Yue He *et al.*,[68] reported that the water solubility of PVA/Agarose based films decreased with increasing anthocyanin content from 3–6%; however, when the anthocyanin content exceeded 6%, the film solubility increased again.

However, upon reinforcement with cellulose fibers at different loadings, the water solubility exhibited a decreasing

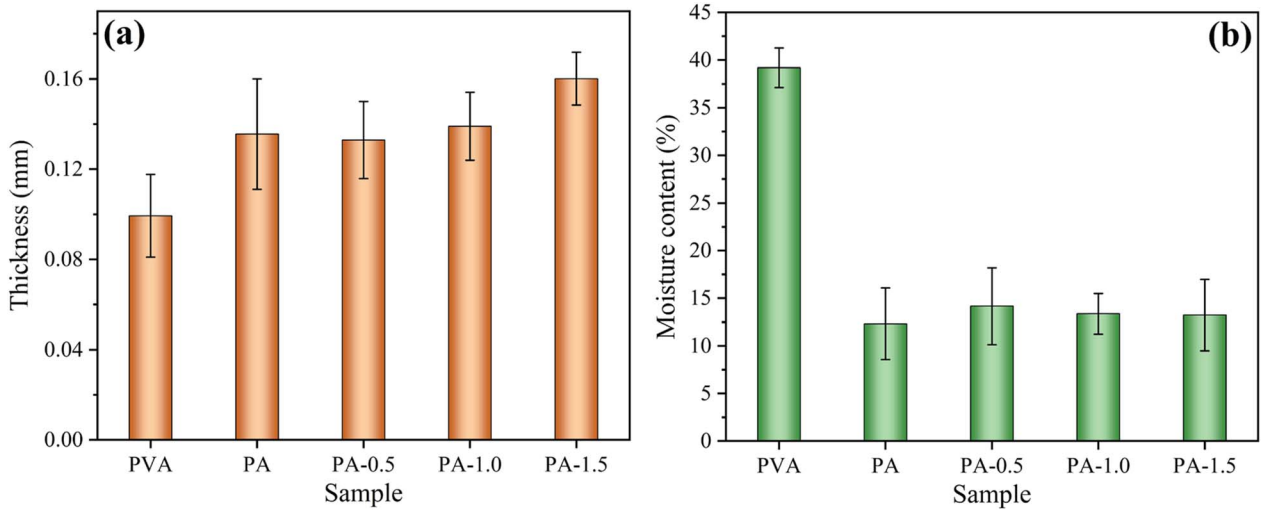

Fig. 12 (a) Thickness and (b) moisture content of PVA film, PVA film with anthocyanin, and films reinforced with different cellulose contents.

trend from 31.33 ± 3.52% to 24.57 ± 1.03%. This reduction was attributed to the formation of hydrogen bonds through interactions between the hydroxyl groups of PVA and cellulose fibers, thereby decreasing the number of free –OH groups in the PVA matrix.[69] In addition, the high crystallinity index of cellulose promoted intermolecular interactions between PVA and cellulose fibers, leading to the formation of a more compact network structure and consequently reducing the solubility of the indicator films.[69] According to the study by Banhisikha Debnath *et al.*,[69] the solubility of PVA films decreased from 29.79 ± 0.53% to 16.67 ± 0.21% as the microcrystalline cellulose content increased from 0 to 5%. Another study indicated that when 2% cellulose was incorporated into a PVA/AgNPs/banana bract extract (BBE) matrix, the solubility reached 3.6 ± 0.27%, which was significantly lower than that of neat PVA (63.0 ± 0.84%).[70] However, when the cellulose content was increased to 5%, the water solubility slightly increased to 4.6 ± 0.15%.[70] These results indicated that the incorporation of cellulose fibers and anthocyanins could either increase or decrease the water solubility of PVA-based indicator films, depending on their content.

3.3.3. Water vapor permeability. Water vapor permeability (WVP) was used to quantitatively evaluate the transmission of water vapor through both surfaces of the films. This parameter was important for determining the moisture barrier properties of the films, thereby assessing their potential applicability in food packaging and preservation. The WVP values of the film samples were presented in Fig. 14.

Compared with the neat PVA film, the PA film showed that the WVP value increased from 1.56 ± 0.24 ($\times 10^{-10}$ g m^{-1} s^{-1} Pa^{-1}) to 3.39 ± 0.20 ($\times 10^{-10}$ g m^{-1} s^{-1} Pa^{-1}) upon the incorporation of anthocyanin. This increase in WVP was attributed to the presence of hydrophilic phenolic hydroxyl groups in the chemical structure of anthocyanin, which increased the number of hydrophilic functional groups in the film matrix.[71] This promoted water absorption, allowing water molecules to diffuse more easily through the film structure.[72] In addition, the incorporation of anthocyanin into the PVA matrix acted as a plasticizer, increasing chain mobility and reducing the compact packing of PVA chains, thereby facilitating water vapor diffusion through the film structure and leading to an increase in WVP.[73] This trend was consistent with results reported by Dan Zheng *et al.*,[74] in which anthocyanin extracted from blueberry and incorporated into a chitosan matrix without cellulose reinforcement exhibited a WVP of 31.62 × 10^{-12} ± 0.31 g (m^{-1} s^{-1} Pa^{-1}), which was significantly higher than that of the neat chitosan film. Another study showed that when anthocyanin extracted from purple sweet potato peel was incorporated into a sodium alginate matrix at contents ranging from 2–8%, the WVP value continuously decreased from 1.91 ± 0.06 to 1.24 ± 0.05 ($\times 10^{-9}$ g m^{-2} s^{-1} Pa^{-1}); however, when the anthocyanin content increased to 10%, the WVP value increased again to 1.34 ± 0.14 ($\times 10^{-9}$ g m^{-2} s^{-1} Pa^{-1}).[75] These studies indicated that the incorporation of anthocyanin could either increase or decrease the WVP of films depending on the type of polymer matrix and the anthocyanin content.

Notably, when cellulose fibers were incorporated at a content of 0.5%, the WVP value further increased. This increase was attributed to the formation of interconnected diffusion pathways within the film structure due to cellulose fiber reinforcement, which facilitated the transport of water vapor through the film.[76] When the cellulose fiber content increased to 1%, the WVP value decreased to 2.95 ± 0.25 ($\times 10^{-10}$ g m^{-1} s^{-1} Pa^{-1}). This phenomenon was explained by the appropriate incorporation of cellulose fibers into the PVA matrix, which improved the structural density of the PA-1.0 film.[77] In addition, the presence of cellulose fibers at an optimal content increased the tortuosity of the diffusion pathways within the PVA matrix, thereby prolonging the diffusion path of water vapor through the film and resulting in a decrease in WVP for the PA-1.0 sample.[78] However, when the cellulose fiber content was further increased to 1.5%, the WVP value increased again. This was attributed to the aggregation of cellulose fibers at higher

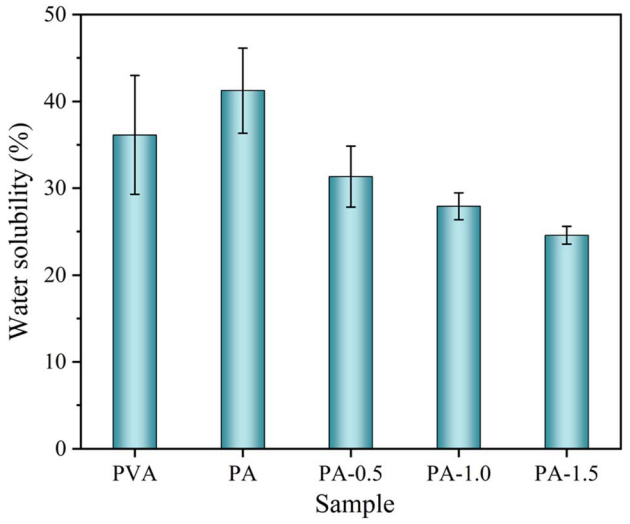

Fig. 13 Water solubility of PVA film, PVA film with anthocyanin, and films reinforced with different cellulose contents.

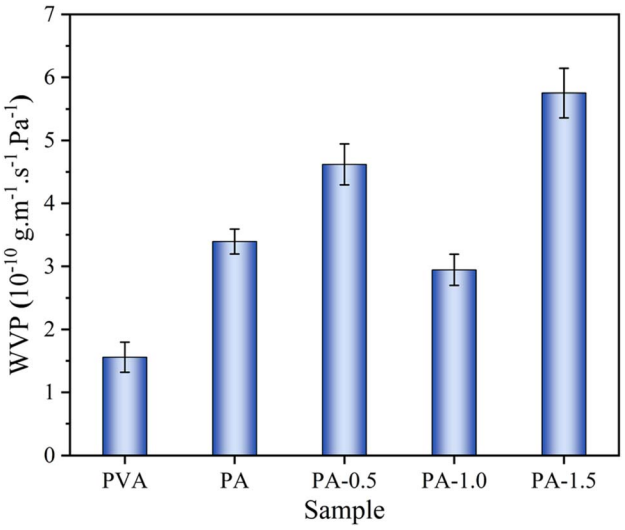

Fig. 14 Water vapor permeability of PVA film, PVA film with anthocyanin, and films reinforced with different cellulose contents.

loading levels, which introduced structural defects within the film matrix and facilitated water vapor diffusion, thereby increasing the WVP value.[77]

These results demonstrated that the cellulose fiber content affected the water vapor permeability of PVA-based films. Furthermore, the presence of cellulose fibers contributed to the formation of diffusion pathways within the film structure, facilitating the transport of water molecules and target gases such as NH_3, thereby enabling faster and more sensitive colorimetric responses.[73] These results indicated that the fabricated films were suitable for application as freshness indicator films for food.

3.3.4. Fourier-transform infrared spectroscopy (FTIR) analysis. The FTIR spectra of PVA-based films incorporated with PPFP extract and various cellulose fibers (CFs) contents were shown in Fig. 15. The FTIR spectrum of neat PVA film displayed a broad band with a maximum absorption peak at 3273 cm^{-1}, assigned to the stretching vibration of (O–H) in the chemical structure of PVA. Furthermore, the absorption peak at 2947 cm^{-1} was characteristic of the stretching vibration of (C–H) in the CH_2 group. The absorption peak at 1644 cm^{-1} observed in all samples corresponded to the bending vibration of (O–H) due to absorbed water. Finally, the peaks at 1416 cm^{-1} and 1086 cm^{-1} were attributed to the bending vibration of (C–H) in the CH_2 group and the stretching vibration of (C–O) in the chemical structure of PVA, respectively.[79] According to the study by Xiuli Wu *et al.*,[79] FTIR spectrum of anthocyanin exhibited characteristic peaks related to polyphenols, including absorption bands at 3374 cm^{-1}, 1610 cm^{-1}, and 1026 cm^{-1}, corresponding to the stretching vibration of (O–H), the stretching vibration of (C=C) in the aromatic ring, and the vibration of (C–H), respectively.

Compared with the FTIR spectrum of neat PVA film, the spectra of films containing anthocyanin-rich extracts from purple passion fruit peel and reinforced with different CFs contents retained the characteristic absorption bands of the PVA matrix. However, changes in peak intensity and peak overlap were clearly observed in the fingerprint region, indicating interactions among the components within the film system. Specifically, the absorption peak at 1038 cm^{-1}, related to the pyranose ring vibration (C–O–C) in the cellulose structure, overlapped with the ether (C–O) stretching of the PVA backbone,[52] thereby confirming the presence of cellulose fibers within the polymer matrix. In addition, the absorption bands observed in the range of 1087–1038 cm^{-1} could also be associated with C–O and C–H vibrations of glycosidic linkages and aromatic structures in anthocyanin compounds.[80,81] A slight decrease in the intensity of the peak around 1087 cm^{-1} was observed after the incorporation of PPFP extract and CFs, which may be related to intermolecular interactions and partial rearrangement of the amorphous regions within the PVA matrix.[82] Notably, no new absorption peaks were detected in the FTIR spectra of the composite films, suggesting that the blending process mainly involved physical interactions rather than the formation of new covalent bonds. This finding agreed with results reported by Jiang *et al.*[52] and Tian *et al.*[83]

3.3.5. X-ray diffraction (XRD) analysis. The XRD patterns shown in Fig. 16 were analyzed to evaluate the effects of PPFP extract and different cellulose contents on the structure of the PVA films. The main diffraction peaks of anthocyanin extracted from purple passion fruit peel appeared at $2\theta = 28.43°$, 31.78°, 40.59°, 50.25°, 56.51°, 58.73°, 66.47°, and 73.80°.[52]

Meanwhile, the XRD pattern of pure PVA film exhibited characteristic diffraction peaks at $2\theta = 19.3°$ and 22.2°, corresponding to the (101) and (200) planes, respectively.[84] Moreover, all films presented diffraction peaks at $2\theta = 19.3°$ and 22.2°, along with a weak peak at 16.2°. The crystallinity index of PVA, PA, PA-0.5, PA-1.0, and PA-1.5 films were 30.38%, 38.75%, 44.00%, 47.13%, and 34.78%, respectively. The incorporation of

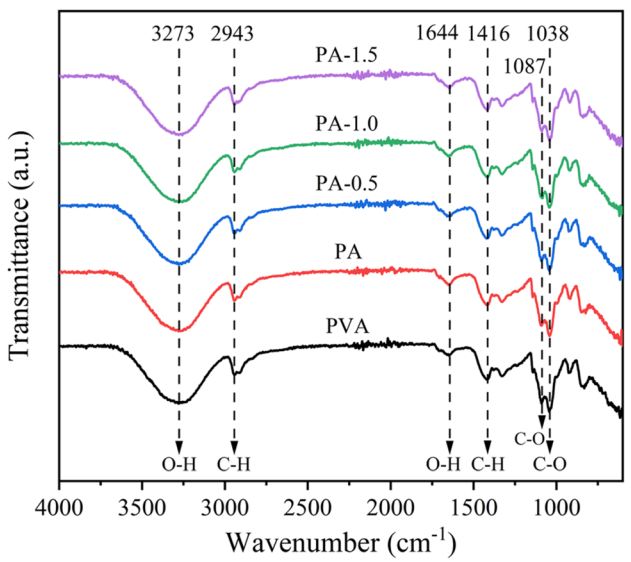

Fig. 15 FTIR spectra of PVA film, PVA film incorporated with anthocyanin, and films reinforced with different cellulose contents.

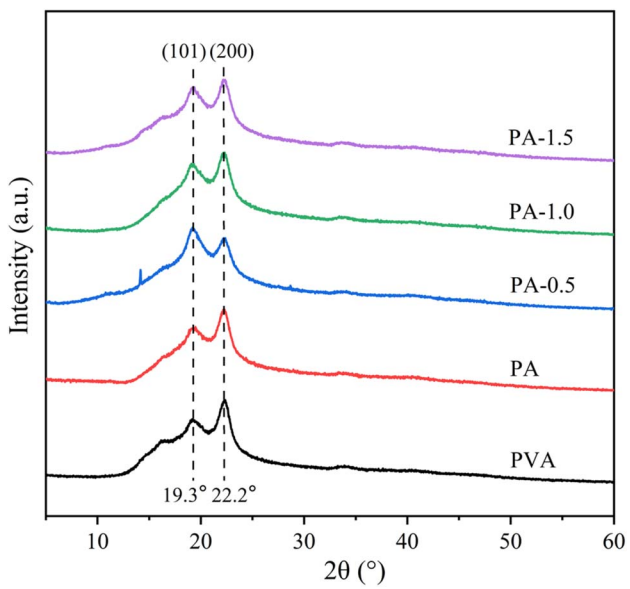

Fig. 16 XRD patterns of PVA film, PVA film with anthocyanin, and films reinforced with different cellulose contents.

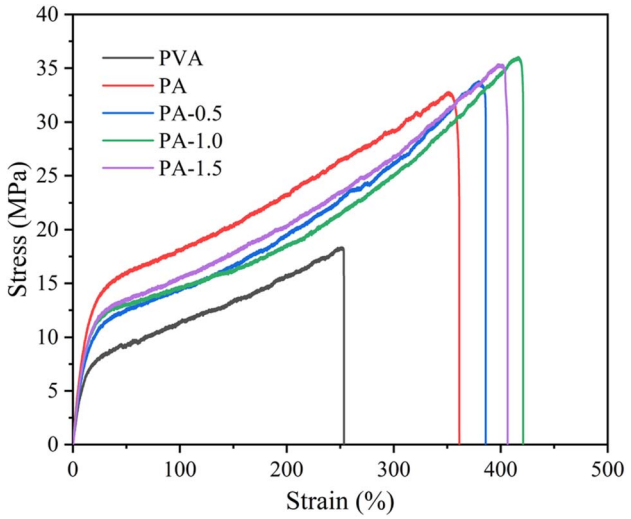

Fig. 17 The stress–strain curves of PVA film, PVA film with anthocyanin, and films reinforced with different cellulose contents.

anthocyanin into the PA film significantly increased the crystallinity index compared with pure PVA. This could be explained by the formation of hydrogen bonds between OH groups in both anthocyanin and PVA, resulting in enhanced crystallinity.[85] Qin *et al.*[85] reported that anthocyanin from Lycium ruthenicum Murr increased the crystallinity of cassava starch-based films. Additionally, in the study by Jiang *et al.*,[52] anthocyanin from passion fruit peel did not significantly affect the crystallinity of films based on Pouteria campechiana seed starch. These findings suggested that the influence of anthocyanins on the crystalline structure of PVA-based films may depend on both the source of anthocyanins and the type of polymer employed.[86]

Furthermore, the interaction among PVA, anthocyanin, and cellulose fibers through hydrogen bonding among –OH groups resulted in a significant increase in the crystallinity index of PA-0.5 and PA-1.0 samples. However, the PA-1.5 sample exhibited a decrease in crystallinity, which could be attributed to excessive CFs content leading to aggregation and hindering the rearrangement of PVA chains, thereby reducing the crystallinity of the PA-1.5 film.[69]

3.3.6. Mechanical properties. The results presented in Fig. 17 and Table 5 indicated that the tensile strength, elongation at break, and Young's modulus of the PA films were higher than those of the neat PVA film. This improvement was attributed to the uniform dispersion of anthocyanin within the PVA matrix and the formation of hydrogen bonds between hydroxyl groups in the chemical structures of anthocyanin and PVA.[81] Consequently, the tensile strength of the films markedly improved, and anthocyanin acted as a plasticizer, enhancing the mobility of PVA chains.[87] In the study conducted by Zhang *et al.*,[24] the addition of anthocyanin from purple sweet potato at 0.5% and 1% (w/v) showed that 0.5% (w/v) significantly improved the tensile strength and elongation at break of PVA/corn starch films, whereas an increase to 1% (w/v) led to a sharp decrease in both properties. Moreover, in the study by Jiang *et al.*,[52] increasing anthocyanin content from 3% to 9% (w/w) significantly reduced the tensile strength while increasing the elongation at break of starch-based films. These results suggested that the interaction between the polymer and anthocyanin could influence the mechanical properties of the films (Tables S7, S9 and S11 of the Supplementary Information), depending on the origin and composition of the anthocyanin.[86]

Furthermore, Table 5 showed the tensile strength of PA films reinforced with CFs. Compared with the unreinforced film, the tensile strength of PA-0.5 reached 29.97 ± 3.66 MPa, PA-1.0 reached 32.21 ± 3.43 MPa, and the highest value was obtained for PA-1.5 at approximately 33.50 ± 2.16 MPa. The ANOVA results indicated that the tensile strength tended to increase as the CFs content increased from 0.5% to 1.5%; however, it was not significantly different from that of PA, as shown in Table S8 of the Supplementary Information. This was explained by the homogeneous dispersion of cellulose in the PVA matrix, which improved stress transfer and reduced local stress concentration, thereby increasing the tensile strength.[69] In addition, Table 5 showed that the elongation at break increased significantly with CFs reinforcement at different contents (Table S10 of the Supplementary Information). All CFs-reinforced films exhibited elongation above 300%, with PA-1.0 achieving the highest value of 404.68 ± 16.95%, approximately 15.77% higher than the unreinforced PA film. This phenomenon was explained by the optimal CFs content in the PVA matrix disrupting some intermolecular and intramolecular interactions within PVA, which enhanced the elongation of the films.[69] Regarding Young's modulus, all CFs-reinforced films exhibited a proportional increase with increasing CFs content from 0.5% to 1.5%. In addition, ANOVA analysis indicated that the differences among films reinforced with different CFs contents were not statistically significant, as shown in Table S12 of the Supplementary Information. Similar results were reported by Debnath *et al.*,[69] who used microcrystalline cellulose (MCC) as a reinforcing agent for PVA films at 1% MCC, no

Table 5 The mechanical parameters of PVA film, PVA film with anthocyanin, and films reinforced with different cellulose contents[a]

Sample	Tensile strength (MPa)	Elongation at break (%)	Young's modulus (MPa)
PVA	21.09 ± 2.53[b]	261.06 ± 6.64[b]	91.72 ± 19.33[a]
PA	30.29 ± 3.60[a]	349.54 ± 14.14[a]	98.96 ± 15.98[a]
PA-0.5	29.97 ± 3.66[a]	363.92 ± 23.68[ac]	91.70 ± 1.36[a]
PA-1.0	32.21 ± 3.43[a]	404.68 ± 16.95[c]	97.05 ± 3.35[a]
PA-1.5	33.50 ± 2.16[a]	382.52 ± 22.89[ac]	99.76 ± 12.72[a]

[a] Different superscript letters within the same column indicate statistically significant differences ($p < 0.05$).

Table 6 Comparison of mechanical properties of PVA-based indicator films

Material	Anthocyanin source	Tensile strength (MPa)	Elongation at break (%)	Young's modulus (MPa)	References
PVA/cellulose fibers/anthocyanin film	Purple passion fruit peel	32.21 ± 1.98	404.68 ± 9.79	97.05 ± 1.94	This study
Cellulose zinc oxide/anthocyanin PVA film	Red cabbage	35 ± 3.6	443.5 ± 30	—	88
PVA/sodium carboxymethyl cellulose/ red cabbage anthocyanins film	Red cabbage	42.785 ± 0.673	38.201 ± 2.390	—	89
PVA/cellulose nanocrystal/ anthocyanins film	Purple cabbage	32.35 ± 1.06	616.36 ± 5.19	34.07 ± 0.42	47
PVA/cellulose/silver nanoparticles/ banana bract extract film	Banana bract	20.4 ± 1.0	168.5 ± 5.0	—	70

significant difference in Young's modulus was observed compared with the neat PVA film, but increasing MCC content to 3% and 5% resulted in a significant increase in Young's modulus. These results indicated that an appropriate CFs content improved the mechanical properties of the films due to good dispersion in the PVA matrix and effective adhesion *via* hydrogen bonding between the two components. The mechanical properties of PVA-based indicator films were summarized in Table 6.

3.3.7. Scanning electron microscope (SEM) analysis. The SEM images of the PVA-based films were presented in Fig. 18. Fig. 18a showed that the neat PVA film exhibited a smooth, homogeneous surface without any observable defects. In contrast, the PA film containing anthocyanin showed a noticeable change in surface morphology, as observed in Fig. 18b. The surface of the PA film became rougher compared to that of the neat PVA film. This phenomenon was attributed to the formation of secondary interactions between anthocyanin and the PVA chains, along with the generation of localized crosslinking points, which resulted in a rougher and more irregular surface of the PA film.[90] For the films reinforced with cellulose fibers at different loadings, the surfaces appeared relatively smoother than that of the PA film. This behavior was associated with the formation of a hydrogen bonding network among the hydroxyl groups of PVA, anthocyanin, and cellulose fibers, thereby creating strong interfacial adhesion between the cellulose fibers and the PVA/anthocyanin matrix.[91] Furthermore, the cellulose fibers were relatively uniformly dispersed within the polymer matrix, and no significant agglomeration was observed on the film surface at fiber loadings of 0.5% and 1.0%, as shown in Fig. 18c and d. However, when the cellulose content increased to 1.5%, pronounced agglomeration on the film surface was observed in Fig. 18e. This could be attributed to the incorporation of a higher amount of cellulose fibers into the PVA/ anthocyanin matrix, which reduced their dispersion capability and led to the formation of large aggregates on the surface.[92]

3.3.8. The color changes of films in different pH buffers. The color changes of films in the pH range from 2 to 12 were presented in Fig. 19. Under acidic conditions (pH 2–4), the films exhibited a deep pink color, which gradually faded as the pH

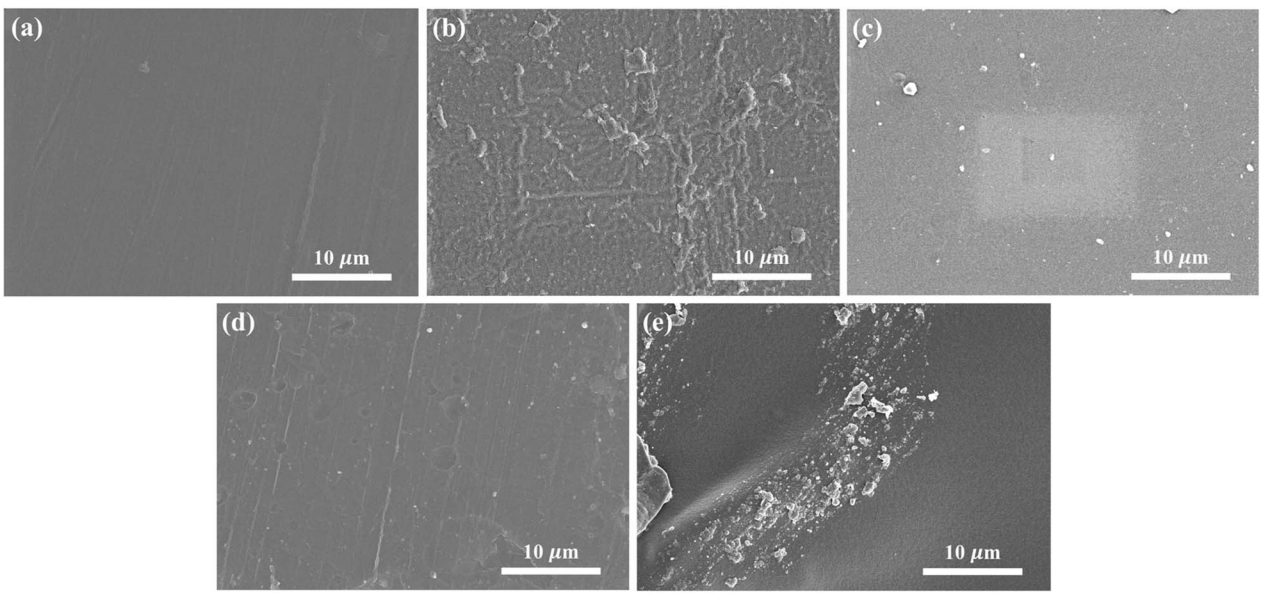

Fig. 18 SEM images of (a) PVA film, (b) PA film, and (c, d, e) films reinforced with different cellulose contents.

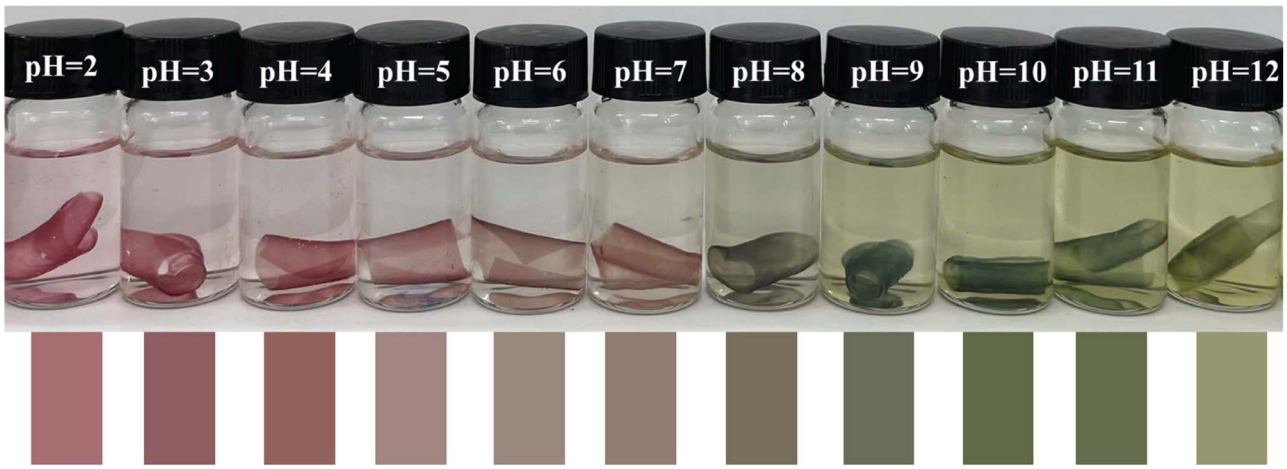

Fig. 19 Color changes of films at to buffer solutions with pH 2–12.

increased. In the neutral pH range (5–7), the color of the films remained nearly unchanged compared with the original state. When the environment shifted from acidic to alkaline, the film color changed noticeably, turning green and gradually deepening as the pH increased from 8 to 11. Under strongly alkaline conditions, anthocyanin in the films began to degrade and gradually turned yellow at pH 12. The observed color changes corresponded to the structural transformations of anthocyanin from flavylium cation (red), carbinol pseudobase (colorless), anionic quinonoidal base (green), to chalcone (yellow) with the shift from acidic to alkaline conditions. The color-changing trend of the films was consistent with the color variations of the PPFP extract shown in Fig. 5a.

3.3.9. Application of film in sensing shrimp freshness. The color changes of the films in pH-sensitive applications for monitoring fresh shrimp during storage at 4 °C were presented in Fig. 20. During storage, protein-rich meat and seafood products degraded to produce volatile nitrogen-based compounds such as ammonia and amines, generated by enzymes and microorganisms. Incorporating anthocyanin into films created pH-sensitive intelligent films, thereby demonstrating the potential of these films as pH indicators. The prepared films exhibited distinct color changes over storage time. At 0 hours, the films were reddish-brown, which gradually faded after 24 hours. At 36 hours, partial discoloration of the films was observed. When the storage time reached 48 hours, the entire film turned brown. At 60 hours, the films began to turn light green, which deepened progressively until 72 and 84 hours. These obvious color changes were easily observed by the naked eye, indicating the freshness of the shrimp during cold

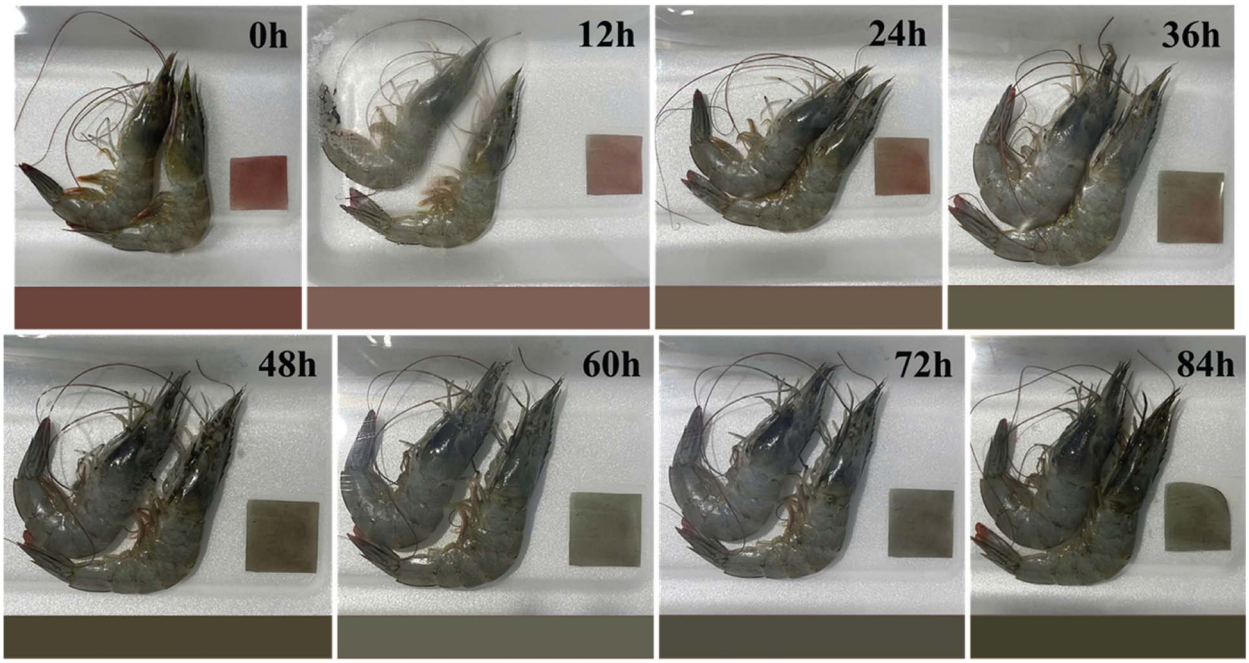

Fig. 20 Color change of the film during the storage of fresh shrimp over extended periods at 4 °C.

storage. Recent studies have also demonstrated the potential application of anthocyanin-based films extracted from plants for monitoring the freshness of meat, shrimp, fish, and seafood.[52,93] These results highlighted the potential application of the films prepared in this study as smart food indicator films.

4. Limitations, scalability and future development

Although this study demonstrated promising potential for food freshness monitoring applications, several limitations remained to be addressed. First, the extraction and washing processes used to isolate cellulose fibers (CFs) from ginger pseudostems required a relatively large amount of water, which posed challenges in terms of sustainability and scalability for practical production. In addition, the color stability of anthocyanin-containing films under prolonged light exposure and extended storage conditions was not comprehensively evaluated, which could affect the reliability of the indicator system in food-packaging applications. Besides that, the freshness-indicating performance of the films was primarily assessed based on visually observable color changes during shrimp storage, whereas quantitative correlations with key physicochemical spoilage indicators such as total volatile basic nitrogen (TVB-N) and pH variation over storage time were not reported.

In addition, the extraction processes for anthocyanins and cellulose fibers at the laboratory scale remain relatively labor- and resource-intensive, involving multiple extraction, washing, and purification steps. These factors may limit the practical feasibility and industrial-scale implementation of the developed materials due to challenges associated with operational cost, process integration, and resource efficiency. Nevertheless, the extraction methods employed in this study are based on relatively established technologies, including ultrasound-assisted extraction and alkaline hydrogen peroxide treatment, which possess recognized potential for industrial adaptation and scalable production.[94,95] Furthermore, the use of abundant and low-cost agricultural by-products as feedstocks may contribute to improving the economic feasibility and sustainability of the proposed intelligent packaging system for future industrial applications.

Therefore, future studies should prioritize the optimization of cellulose fiber extraction from ginger pseudostems to improve product quality while reducing water, chemical, and energy consumption during processing. In addition, optimization of the fabrication process for smart films used as freshness indicators for fresh food products by employing response surface methodology (RSM) based on influential factors, such as PVA solution concentration, cellulose fiber content, and anthocyanin concentration, has also been considered necessary. In parallel, enhancing the stability of anthocyanins within films through strategies such as encapsulation or chemical modification should be considered to improve color durability under real storage conditions. Moreover, the indicator performance of the PVA-based films should be systematically evaluated under diverse environmental conditions, including varying humidity, light exposure, and storage regimes ranging from frozen to ambient temperatures, across different food matrices to assess their broader applicability. Moreover, the antioxidant activities of the extract and anthocyanin-based smart films have needed to be evaluated using DPPH (2,2-Diphenyl-1-picrylhydrazyl) and ABTS (2,2′-azinobis-(3-ethyl-benzothiazoline-6-sulfonic acid)) radical scavenging assays. Finally, comprehensive analyses of key physicochemical parameters such as TVB-N, biodegradability, food safety, and compatibility of the indicator films with existing packaging systems are essential to facilitate the transition from laboratory-scale research to practical applications.

5. Conclusions

In this study, anthocyanins were successfully extracted from purple passion fruit peel using an ultrasonic-assisted extraction method, achieving a maximum yield of 1.53 mg C3G per g DW under optimal conditions. The degradation of anthocyanins followed first-order kinetics, with the degradation rate constant increasing from 0.015 day^{-1} at 4 °C to 0.117 day^{-1} at room temperature, while the corresponding half-life decreased from 46.21 to 5.92 days, indicating the significant effect of storage temperature on anthocyanin degradation. Furthermore, cellulose fibers extracted from ginger pseudostems exhibited a crystallinity index of 74.65%, good thermal stability, and a smooth fiber surface. In addition, the incorporation of anthocyanins and cellulose fibers into the PVA matrix led to changes in the structure and physicochemical properties of the indicator films. Specifically, the film thickness increased from 0.099 to 0.160 mm, while the moisture content and water solubility decreased to 13.22% and 24.57 ± 1.03%, respectively. Moreover, reinforcement with 1.0 wt% cellulose fibers improved the water vapor permeability of the films. At the same time, the mechanical properties were enhanced, with the tensile strength reaching 32.21 ± 3.43 MPa, the elongation at break increasing to 404.68 ± 16.95%, and Young's modulus reaching 97.05 ± 3.35 MPa. Finally, the fabricated indicator films exhibited distinct color changes in response to pH variation and shrimp freshness, with a clear transition from pinkish-brown to green corresponding to the spoilage process. These results demonstrated that the incorporation of anthocyanins extracted from purple passion fruit peel and cellulose fibers derived from ginger pseudostems into the PVA matrix not only improved the physicochemical properties of the films but also enabled real-time monitoring of fresh food quality, highlighting their strong potential for applications in intelligent food packaging.

Author contributions

Nguyen Chi Thanh: conceptualization, data curation, formal analysis, investigation, methodology, supervision, validation, visualization, writing – original draft, writing–review& editing. Pham Nguyen Hong Nhu: data curation, formal analysis, investigation, methodology, validation, visualization, writing–original draft, writing–review& editing. Nguyen Quoc Dat: formal analysis, investigation, writing–review & editing. Bui Phuong Dong: formal analysis, writing–review & editing. Nguyen Thanh Huy: formal analysis. Nguyen Bui Anh Duy: formal analysis. Nguyen Tue Anh: formal analysis.

Conflicts of interest

There are no conflicts to declare.

Data availability

The supporting data has been provided as part of the supplementary information (SI). Supplementary information is available. See DOI: https://doi.org/10.1039/d6ra03420a.

Acknowledgements

We gratefully acknowledge financial support from Ho Chi Minh City University of Technology and Engineering (HCM-UTE). This study belongs to project grant no: T2026-23.

References

1 S. Chen, M. Wu, P. Lu, L. Gao, S. Yan and S. Wang, *Int. J. Biol. Macromol.*, 2020, **149**, 271–280.
2 P. A. V. Freitas, R. R. A. Silva, T. V. de Oliveira, R. R. A. Soares, N. S. Junior, A. R. F. Moraes, A. C. d. S. Pires and N. F. F. Soares, *LWT*, 2020, **132**, 109780.
3 N. N. T. Tien, H. T. Nguyen, N. L. Le, T. T. Khoi and A. Richel, *Food Packag. Shelf Life*, 2023, **37**, 101084.
4 X. Zhang, X. Chen, J. Dai, H. Cui and L. Lin, *Food Packag. Shelf Life*, 2023, **40**, 101215.
5 X. Zhao, H. Zhang, H. Xiang, D. Yu, M. Gao, R. Yan and D. Zhang, *Food Biosci.*, 2024, **57**, 103519.
6 I. Mutmainna, D. Tahir, P. L. Gareso and S. Suryani, *Int. J. Biol. Macromol.*, 2025, **313**, 144205.
7 R. Thokchom and G. Mandal, *J. Agric. Eng. Food Technol.*, 2017, **4**, 27–30.
8 L. C. R. dos Reis, E. M. P. Facco, M. Salvador, S. H. Flôres and A. de Oliveira Rios, *J. Food Sci. Technol.*, 2018, **55**, 2679–2691.
9 S. Sakulrang, M. Razem, N. Mohammadi and D. Granato, *Future Foods*, 2025, **11**, 100599.
10 N. Mohammadi, M. Franchin, C. Girotto Pressete, L. Maria Greggi Antunes and D. Granato, *Food Res. Int.*, 2024, **196**, 115128.
11 M. Xu, D. Fang, B. M. Kimatu, L. Lyu, W. Wu, F. Cao and W. Li, *Food Control*, 2024, **162**, 110431.
12 P. Zeng, X. Chen, Y.-R. Qin, Y.-H. Zhang, X.-P. Wang, J.-Y. Wang, Z.-X. Ning, Q.-J. Ruan and Y.-S. Zhang, *Food Res. Int.*, 2019, **126**, 108604.
13 Food and Agriculture Organization of the United Nations, *FAOSTAT database*, https://www.fao.org/faostat/en/#compare, accessed February, 2025.
14 Research and Markets, Ginger Oil Market - Forecasts from 2025 to 2030, https://www.researchandmarkets.com/reports/5649144/ginger-oil-market-forecasts-from-2025-to-2030, accessed February, 2025.
15 N. Inthalaeng, Y. Gao, J. Remón, T. I. J. Dugmore, M. Z. Ozel, A. Sulaeman and A. S. Matharu, *RSC Sustainability*, 2023, **1**, 213–223.
16 M. M. Giusti and R. E. Wrolstad, *Curr. Protoc.*, 2001, **00**, F1.2.1–F1.2.13.
17 T. N. Pham, X. T. Le, V. T. Pham and H. T. Le, *Heliyon*, 2022, **8**, e09518.
18 T. G. Oliveira, G. L. A. Makishi, H. N. M. Chambi, A. M. Q. B. Bittante, R. V. Lourenço and P. J. A. Sobral, *Ind. Crops Prod.*, 2015, **67**, 355–363.
19 P. A. V. Freitas, L. G. Santana, C. González-Martínez and A. Chiralt, *Carbohydr. Polym. Technol. Appl.*, 2024, **7**, 100491.
20 L. Segal, J. Creely Jr, A. E. Martin Jr and C. M. Conrad, *Text. Res. J.*, 1959, **29**, 786–794.
21 F. Yudhanto, V. Yudha, H. S. B. Rochardjo, C. Budiyantoro, A. Khan, A. M. Asiri and M. J. M. Ridzuan, *Int. J. Eng.*, 2024, **37**, 94–103.
22 S. Khan, Z. Bao, J. Wang, X. Zhou, Y. Ding, W. Cheng and S. Liu, *Food Hydrocolloids*, 2025, **171**, 111788.
23 Z. Xie, Q. Xiong, Y. Fang, Q. Zhang, W. Liang, J. Cheng, W. Shang, W. Zhao and J. Zhao, *ACS Sustain. Chem. Eng.*, 2023, **11**, 9868–9879.
24 K. Zhang, T.-S. Huang, H. Yan, X. Hu and T. Ren, *Int. J. Biol. Macromol.*, 2020, **145**, 768–776.
25 H. Jiang, W. Zhang, Y. Pu, L. Chen, J. Cao and W. Jiang, *Food Chem.*, 2023, **404**, 134444.
26 H. Yong, J. Liu, J. Kan and J. Liu, *Int. J. Biol. Macromol.*, 2022, **211**, 238–248.
27 G. L. de Barros, F. T. S. Silva, R. S. Teixeira, J. G. Wagner, C. V. Rombaldi, M. Vizzotto, A. Ubeyitogullari and L. Nora, *Int. J. Food Prop.*, 2024, **27**, 1315–1346.
28 T. Belwal, H. Huang, L. Li, Z. Duan, X. Zhang, H. Aalim and Z. Luo, *Food Chem.*, 2019, **297**, 124993.
29 T. Taghavi, H. Patel and R. Rafie, *Plants*, 2023, **12**, 1833.
30 S. Kim, H. Son, S. Y. Pang, J. J. Yang, J. Lee, K. H. Lee, J. H. Lee, C. Park and H. Y. Yoo, *Processes*, 2023, **11**, 72.
31 K. Kaderides, L. Papaoikonomou, M. Serafim and A. M. Goula, *Chem. Eng. Process.*, 2019, **137**, 1–11.
32 M. Lianza, L. Marincich and F. Antognoni, *Antioxidants*, 2022, **11**, 2169.
33 Z. Zhou and D. Yang, *Food Chem.:X*, 2022, **15**, 100419.
34 T. Ahmed, M. R. Rana, M. A. Hossain, S. Ullah and M. Suzauddula, *Biomass Convers. Biorefin.*, 2023, **14**, 28985–28999.
35 J. P. Maran, V. Sivakumar, K. Thirugnanasambandham and R. Sridhar, *J. Food Sci. Technol.*, 2015, **52**, 3617–3626.
36 T. T. Tran, A. T. Nguyen, T. N. H. Le, T. T. N. Dinh, T. N. M. Ngo, T. B. T. Nguyen, Q. P. Ho, V. H. T. Doan and V. N. H. Nguyen, *CTU J. Innov. Sustain. Dev.*, 2025, **17**, 59–68.
37 X. Zhang, S. Wang, Q. Wu, M. Battino, F. Giampieri, W. Bai and L. Tian, *Food Chem.:X*, 2022, **16**, 100476.
38 T.-B. Zou, M. Wang, R.-Y. Gan and W.-H. Ling, *Int. J. Mol. Sci.*, 2011, **12**, 3006–3017.
39 C. T. Nthimole, T. Kaseke and O. A. Fawole, *Processes*, 2024, **12**, 2444.
40 B. R. Albuquerque, J. Pinela, C. Pereira, R. C. Calhelha, I. Oliveira, S. Heleno, M. B. P. P. Oliveira and L. Barros, *Biomass Convers. Biorefin.*, 2025, **15**, 1027–1040.
41 R. Mattioli, A. Francioso, L. Mosca and P. Silva, *Molecules*, 2020, **25**, 3809.
42 B. Enaru, G. Dretcanu, T. D. Pop, A. Stanila and Z. Diaconeasa, *Antioxidants*, 2021, **10**, 1967.

43 Z. Cai, Z. Qu, Y. Lan, S. Zhao, X. Ma, Q. Wan, P. Jing and P. Li, *Food Chem.*, 2016, **197**, 266–272.
44 N. Zahed, R. Esmaeilzadeh Kenari and R. Farahmandfar, *Food Sci. Nutr.*, 2023, **11**, 3780–3787.
45 N. B. Ma, N. N. T. Tien, L. T. K. Vu, N. M. N. Ton and N. L. Le, *J. Agric. Food Res.*, 2024, **18**, 101507.
46 A. C. Pedro, D. Granato and N. D. Rosso, *Food Chem.*, 2016, **191**, 12–20.
47 S. A. Amer, H. S. Al-Khalaifah, A. Gouda, A. Osman, N. I. A. Goda, H. A. Mohammed, M. I. M. Darwish, A. M. Hassan and S. K. A. Mohamed, *Antioxidants*, 2022, **11**, 544.
48 O. Zannou, I. Koca, R. Tahergorabi and S. A. Ibrahim, *Ind. Crops Prod.*, 2025, **230**, 121069.
49 J. Tan, Q. Li, H. Xue and J. Tang, *J. Food Sci.*, 2020, **85**, 3731–3744.
50 D. Ryu and E. Koh, *Food Chem.*, 2018, **261**, 260–266.
51 Y.-W. Zhao, C.-K. Wang, X.-Y. Huang and D.-G. Hu, *Plant Signaling Behav.*, 2021, **16**, 1987767.
52 H. Jiang, W. Zhang and W. Jiang, *Food Hydrocolloids*, 2023, **138**, 108477.
53 J. Herrera-Ramirez, N. Meneses-Marentes and M. P. Tarazona Díaz, *J. Food Meas. Charact.*, 2020, **14**, 185–193.
54 A. Sinela, N. Rawat, C. Mertz, N. Achir, H. Fulcrand and M. Dornier, *Food Chem.*, 2017, **214**, 234–241.
55 S. Fong-in, T. Prommajak, W. Chartarrayawadee and P. Khwanchai, *J. Food Sci. Technol.*, 2025, 1–12.
56 N. E. Fitriana, A. Suwanto, T. H. Jatmiko, S. Mursiti and D. J. Prasetyo, *IOP Conf. Ser.: Earth Environ. Sci.*, 2020, **462**, 012053.
57 R. Ramful, *J. Mater. Sci.: Mater. Eng.*, 2024, **19**, 50.
58 G. T. Melesse, F. G. Hone and M. A. Mekonnen, *Adv. Mater. Sci. Eng.*, 2022, **2022**, 1712207.
59 V. Raju, R. Revathiswaran, K. S. Subramanian, K. T. Parthiban, K. Chandrakumar, E. V. Anoop and C. J. Chirayil, *Sci. Rep.*, 2023, **13**, 1199.
60 M. Le Troedec, D. Sedan, C. Peyratout, J. P. Bonnet, A. Smith, R. Guinebretiere, V. Gloaguen and P. Krausz, *Composites, Part A*, 2008, **39**, 514–522.
61 C.-M. Popescu, M.-C. Popescu, G. Singurel, C. Vasile, D. S. Argyropoulos and S. Willfor, *Appl. Spectrosc.*, 2007, **61**, 1168–1177.
62 N. Sharma, B. J. Allardyce, R. Rajkhowa and R. Agrawal, *Sci. Rep.*, 2023, **13**, 16327.
63 M. A. Masanabo, J. T. Keränen, S. S. Ray and M. N. Emmambux, *J. Sci. Food Agric.*, 2025, **105**, 1375–1384.
64 H. M. Zendrato, N. Masruchin, S. Nikmatin and N. J. Wistara, *J. Ind. Eng. Chem.*, 2024, **131**, 376–387.
65 F. A. Zaki, I. Abdullah and I. Ahmad, *Int. J. Mater. Eng. Innovation*, 2014, **5**, 48–60.
66 Z. Xiao, C. Liu, X. Rong, D. E. Sameen, L. Guo, J. Zhang, X. Chu, M. Chen, Y. Liu and W. Qin, *Int. J. Biol. Macromol.*, 2023, **253**, 127343.
67 C. Amara, A. El Mahdi, P. K. Akman, R. Medimagh, F. Tornuk and K. Khwaldia, *Food Sci. Nutr.*, 2023, **11**, 5102–5113.
68 Y. He, B. Li, J. Du, S. Cao, M. Liu, X. Li, D. Ren, X. Wu and D. Xu, *Int. J. Biol. Macromol.*, 2022, **201**, 203–215.
69 B. Debnath, P. Duarah and M. K. Purkait, *ACS Sustainable Resour. Manage.*, 2024, **1**, 2518–2529.
70 S. Maroor and V. Badalamoole, *Int. J. Biol. Macromol.*, 2025, **332**, 148547.
71 N. Guo, M. Song, W. Liu, F. Zhang and G. Zhu, *PLoS One*, 2023, **18**, e0290650.
72 Y. Qi and Y. Li, *Polymers*, 2024, **16**, 495.
73 J. Sun, L. Zeng, Y. Tao, H. Lan, S. Kraithong, J. Gao, S. Deng and J. W. C. Wong, *J. Food Process Eng.*, 2025, **48**, e70283.
74 D. Zheng, S. Cao, D. Li, Y. Wu, P. Duan, S. Liu, X. Li, X. Zhang and Y. Chen, *Int. J. Biol. Macromol.*, 2024, **264**, 130692.
75 M. Zhao, M. Nuerjiang, X. Bai, J. Feng, B. Kong, F. Sun, Y. Li and X. Xia, *Int. J. Biol. Macromol.*, 2022, **216**, 361–373.
76 R. H. R. Hashim, A. A. N. Gunny, M. J. Gidado, S. S. Ting, Y. Y. Fong, S. Pareek and N. H. Jamil, *J. Food Sci. Technol.*, 2025, 1–9.
77 Y. Xie, P. Cai, X. Cao and Y. Pan, *Ind. Crops Prod.*, 2024, **207**, 117768.
78 M. H. Salim, Y. Abdellaoui, A. Ait Benhamou, E.-H. Ablouh, M. El Achaby and Z. Kassab, *Cellulose*, 2022, **29**, 5117–5135.
79 X. Wu, X. Yan, J. Zhang, X. Wu, M. Luan and Q. Zhang, *LWT*, 2024, **194**, 115818.
80 W. Fu, S. Li, H. Helmick, B. R. Hamaker, J. L. Kokini and L. Reddivari, *Foods*, 2023, **12**, 1846.
81 L. Ren, S. Yang, N. Wu and J. Xu, *Int. J. Biol. Macromol.*, 2023, **253**, 126800.
82 L. Li, W. Wang, M. Zheng, J. Sun, Z. Chen, J. Wang and Q. Ma, *Carbohydr. Polym.*, 2023, **301**, 120352.
83 Y. Tian, P. Zhu, M. Zhou, Y. Lin and F. Cheng, *J. Wuhan Univ. Technol. Mater. Sci. Ed.*, 2020, **35**, 825–831.
84 W. Yang, G. Qi, J. M. Kenny, D. Puglia and P. Ma, *Polymers*, 2020, **12**, 1364.
85 Y. Qin, Y. Liu, H. Yong, J. Liu, X. Zhang and J. Liu, *Int. J. Biol. Macromol.*, 2019, **134**, 80–90.
86 T. T. T. Nguyen, N. L. Q. Truong, T. N. Q. Chiem, L. D. P. Truong, T. T. T. Nguyen and T. V. Tran, *Int. J. Biol. Macromol.*, 2025, **319**, 145436.
87 L. Xue Mei, A. Mohammadi Nafchi, F. Ghasemipour, A. Mat Easa, S. Jafarzadeh and A. A. Al-Hassan, *Int. J. Biol. Macromol.*, 2020, **164**, 4603–4612.
88 N. K. V, M. Badawi, J. Parameswaranpillai, H. K, A. L. Abraham, P. M. S. Begum and M. Dominic C D, *Sustainable Chem. Pharm.*, 2025, **45**, 102033.
89 D. Liu, Z. Cui, M. Shang and Y. Zhong, *Food Packag. Shelf Life*, 2021, **28**, 100641.
90 T. Gümüş, Y. Henden and D. D. A. Kamer, *J. Sci. Food Agric.*, 2026, DOI: 10.1002/jsfa.70618.
91 S. Van Nguyen and B.-K. Lee, *Cellulose*, 2023, **30**, 1697–1716.
92 H. C. Oyeoka, C. M. Ewulonu, I. C. Nwuzor, C. M. Obele and J. T. Nwabanne, *J. Bioresour. Bioprod.*, 2021, **6**, 168–185.
93 Z. Guo, X. Ge, W. Li, L. Yang, L. Han and Q.-l. Yu, *Food Hydrocolloids*, 2021, **119**, 106751.
94 V. H. Cauduro, G. Gohlke, N. W. da Silva, A. G. Cruz and E. M. M. Flores, *Curr. Opin. Chem. Eng.*, 2025, **48**, 101120.
95 M. C. Ho, V. Z. Ong and T. Y. Wu, *Renewable Sustainable Energy Rev.*, 2019, **112**, 75–86.